



**Particle-In-Cell Code with Monte Carlo Collisions
for ECR Ion Sources Simulation**

Igor Rudskoy

Institute for Theoretical and Experimental Physics,
Moscow, Russia

Introduction

In accordance with theoretical consideration [Hockney] an adequate modeling of plasma by the particle in cell method (PIC) enforces to meet at least the following conditions:

- $\omega\tau \leq 2$
- $h \leq \lambda_d$
- $N_p \lambda_d \gg L$
- $L \gg \lambda_d$

Here ω is plasma frequency, λ_d - Debye radius, L - the size of simulated region, τ , h – time and space steps, N_p - the number of particles.

For typical hydrogen ECRIS parameters ($L \approx 10\text{cm}$, $T_e \approx 10\text{eV}$, $n_e \approx 10^{13} \text{ cm}^{-3}$) these give

$$\lambda_d \approx 7.5 \cdot 10^{-4} \text{ cm}$$

$$\omega \approx 1.26 \cdot 10^{11} \text{ s}^{-1}$$

From which we have (the second and third conditions):

the number of mesh points

$$N_g \geq 14000$$

the number of particles

$$N_p \gg 14000$$

and the time step

$$\tau \leq 0.8 \cdot 10^{-11} \text{ s}$$

So to meet these requirements we need at least 10^5 steps for calculation of 1mks of behavior of plasma which is simulated at least by $N_p \approx 10^5$ particles (in 1D approximation) on the mesh with $N_g \approx 2 \cdot 10^4$ points. 2D approximation brings about

$$N_g \approx 4 \cdot 10^8$$

$$N_p \approx (2 \div 3) \cdot 10^9$$

3D simulation in this case is hardly possible ($N_p > 10^{13}$). One should keep in mind that mean execution time of a simple arithmetic operation on 3.2GHz Xeon equals to about 10^{-8} second and $\approx 10^{-7}$ – for trigonometric and exponential operations (For the reference: one day is equal to $8.64 \cdot 10^4$ seconds only).

But since

$$N_g \sim L \sqrt{Z n_e / T_e}, \quad \omega \sim \sqrt{n_e},$$

the requirements will be much more moderate for modeling of plasma of heavy ion ECR sources ($Z \approx 15 \div 25$, $T_e \approx 10\text{keV}$, $n_e \approx 10^{10} \text{ cm}^{-3}$) where

$$\lambda_d \approx 0.15 - 0.2 \text{ cm}$$

$$\omega \approx 5 \cdot 10^9 \text{ s}^{-1}$$

Respectively

$$N_g \approx 50 \div 100$$

and $5 \cdot 10^3$ steps is necessary to simulate 1 mks. In this case even 3D modeling ($N_g \approx 10^5$, $N_p \approx 5 \cdot 10^5$) looks achievable.

Fortunately, even at the worst case (cold dense plasma) the maximal value of collision rates (for the most frequent elastic Coulomb collisions) does not exceed 10^9 s^{-1} . Therefore it is

the value of plasma frequency that will determine a time step in a PIC code taking into account particle collisions.

Because of the high resources consumption the development of that PIC code to simulate plasma behavior in ECRIS was decided to start with the simplest 1D version increasing the number of dimension as the code is debugged and tested.

1D PIC code without collisions

In this case the behavior of plasma is described by Vlasov equation for particle distribution function f :

$$\frac{\partial f}{\partial t} + v \frac{\partial f}{\partial x} + \frac{F}{m} \frac{\partial f}{\partial v} = 0 \quad (*)$$

Where the force F is determined by electrostatic interaction:

$$F = qE = -q\nabla\phi \quad (**)$$

$$\nabla^2\phi = -4\pi\rho \quad (***)$$

Here v , q are the velocity and charge of the particles respectively. The charge density ρ can be defined by the equation

$$\rho(x, t) = q \int f(x, v, t) dv + \rho_0$$

in case when only one sort of particle is taken into account and another one is considered as neutralizing background with density ρ_0 or

$$\rho(x, t) = \sum_i q_i \int f_i(x, v, t) dv$$

when the above equation for distribution function (*) is solving for each sort of charged particles. (Hereafter index i is attributed to the particles, k - to the grid points, n – to the time slices).

The essence of PIC modeling is substitution of the equation (*) for the equation of its characteristic. Since the distribution function is conserved along particle trajectories:

$$f(x', v', t') = f(x, v, t)$$

where (x', v') and (x, v) are connected by motion equations of the particles:

$$x' = x + \int_t^{t'} v dt \quad v' = v + \int_t^{t'} \frac{F}{m} dt$$

we will divide the phase space involved into N_p meshes (points), where each point i represents i -th volume of the phase space corresponding to

$$N_s = \int f dx dv$$

particles, and solve motion equation for these points:

$$\frac{dx_i}{dt} = v_i \quad m \frac{dv_i}{dt} = F(x_i)$$

For finite-difference approximation of the last equations the well known explicit leapfrog algorithm is used:

$$x_i^{n+1} - x_i^n = v_i^{n+1/2} dt$$

$$v_i^{n+1/2} - v_i^{n-1/2} = \frac{F(x_i^n)}{m} dt$$

To measure the force $F = qE$ acting on the particles the physical area is divided into N_g cells of the size h . So that the equations (**) and (***) move to

$$\frac{\varphi_{k+1} - 2\varphi_k + \varphi_{k-1}}{h^2} = -4\pi\rho_k$$

$$E_k = \frac{\varphi_{k-1} - \varphi_{k+1}}{2h}$$

Here the charge density ρ_k in the grid cell k is defined by the equation

$$\rho_k = \rho(x_k) = \frac{qN_s}{h} \sum_{i=1}^{N_p} W(x_i - x_k) + \rho_0$$

where $W(x)$ is a so-called charge assignment (or weighting) function. The different kinds of this function will be discussed later.

The force on the particle interpolated from an electric field on the mathematical grid can be written as follows

$$F_i = F(x_i) = qN_s \sum_{k=1}^{N_g} W(x_i - x_k) E_k$$

where the same weighting function W is used to eliminate the self-force interaction and ensure conservation of momentum [Hockney].

In the beginning we will simulate only electron fraction of plasma considering plasma ions as neutralizing background with the charge density ρ_0 .

Thus the following finite-difference equations are to be solved at this stage:

1. Charge weighting:

$$\rho_k^n = \frac{qN_s}{h} \sum_{i=1}^{N_p} W(x_i^n - x_k) + \rho_0$$

2. Poisson equation:

$$\frac{\varphi_{k+1}^n - 2\varphi_k^n + \varphi_{k-1}^n}{h^2} = -4\pi\rho_k^n$$

3. Field equation:

$$E_k^n = \frac{\varphi_{k-1}^n - \varphi_{k+1}^n}{2h}$$

4. Force weighting:

$$F_i^n = qN_s \sum_{k=1}^{N_g} W(x_i^n - x_k) E_k^n$$

5. Motion equations:

$$\frac{v_i^{n+1/2} - v_i^{n-1/2}}{dt} = \frac{F_i^n}{N_s m_e}$$

$$\frac{x_i^{n+1} - x_i^n}{dt} = v_i^{n+1/2}$$

To reduce the number of computing operation the standard dimensionless units will be used during calculation:

$$x' = x/h \quad t' = t/dt$$

$$v' = vdt/h \quad a' = adt^2/h$$

$$E'_k = \frac{qdt^2}{m_e h} E_k^n$$

$$\varphi'_k = -\frac{qdt^2}{2m_e h^2} \varphi_k^n$$

$$\rho_k^m = \frac{2\pi q dt^2}{m_e} \rho_k^n$$

In these units the above equation set will look as follows:

$$\rho_k^m = \frac{\omega_p^2 dt^2}{2} \left[\sum_{i=1}^{N_p} \frac{W(x_i^m - x_k)}{N_c} - 1 \right]$$

$$\varphi_{k-1}^m - 2\varphi_k^m + \varphi_{k+1}^m = \rho_k^m$$

$$E_k^m = \varphi_{k+1}^m - \varphi_{k-1}^m$$

$$a_i^m = \sum_{k=1}^{N_g} W(x_i^m - x_k) E_k^m$$

$$v_i^{m+1/2} - v_i^{m-1/2} = a_i^m$$

$$x_i^{m+1} - x_i^m = v_i^{m+1/2}$$

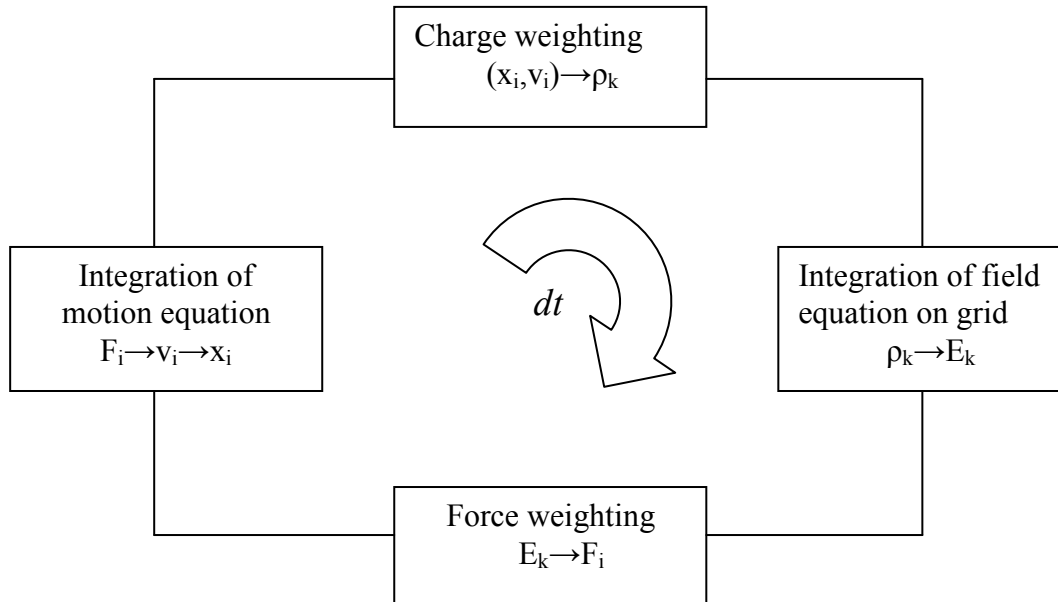
Here ω_p is a plasma frequency:

$$\omega_p = \sqrt{\frac{4\pi q^2 n}{m_e}}$$

($n=n_e=n_i$ is plasma density), and N_c is:


$$N_c = \frac{\rho_0 h}{q N_s}$$

The simplified computing sequence can be presented as



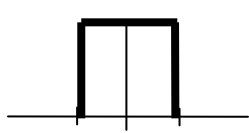
Three different interpolating (weighting) function for charge and force were under consideration:

1. Zero-order scheme Nearest Grid Point (NGP):



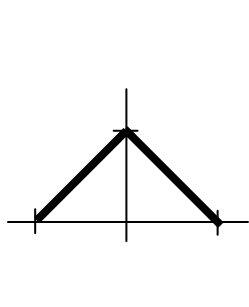
$$W(x) = \begin{cases} 1 & \text{if } |x| \leq h/2 \\ 0 & \text{in another case} \end{cases}$$

2. First-order scheme Cloud In Cell (CIC)



$$W(x) = \begin{cases} 1 - \frac{|x|}{h} & \text{if } |x| \leq h \\ 0 & \text{in another case} \end{cases}$$

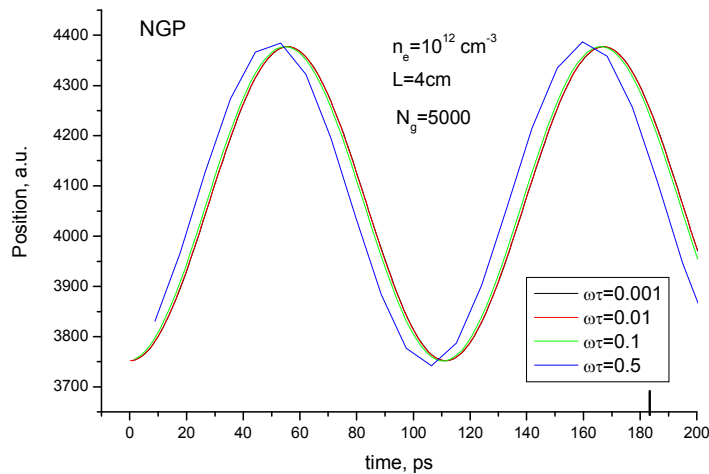
3. Second-order scheme Triangle Shaped Cloud (TSC) ([Birdsall] unlike [Hockney] treats it as a scheme of the first-order of accuracy)



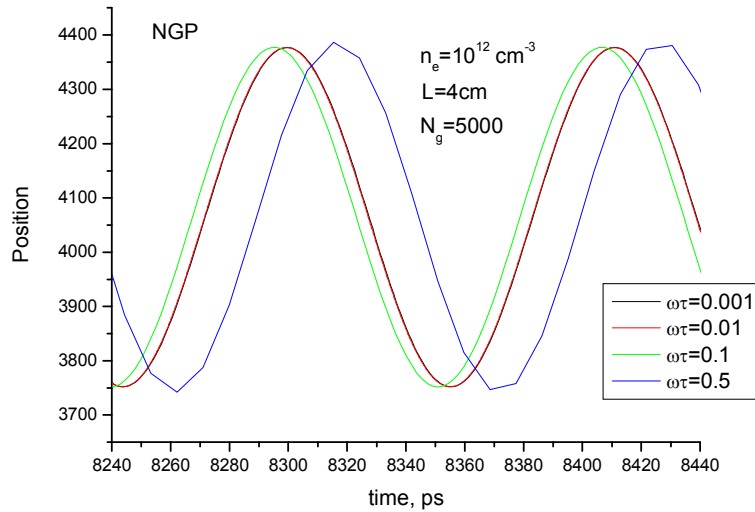
$$W(x) = \begin{cases} \frac{3}{4} - \left(\frac{x}{h}\right)^2 & \text{if } |x| \leq h/2 \\ \frac{1}{2} \left(\frac{3}{2} - \frac{|x|}{h}\right)^2 & \text{if } h/2 \leq |x| \leq 3h/2 \\ 0 & \text{in another case} \end{cases}$$

As the first test of the code developed the conventional two-particle test was run. (Two particles should oscillate with frequency ω_p for any nonzero initial distance between them.) Because we are interested in simulation of many thousands of plasma oscillations and the algorithm of integration of motion equations used in this code does not save a phase of oscillation we will consider mainly the time steps satisfying more stringent requirements $\omega\tau \leq 0.1$

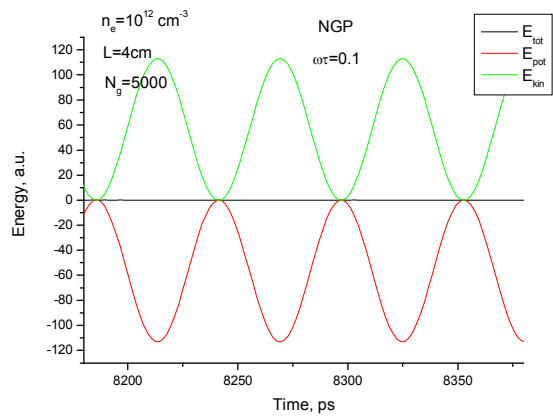
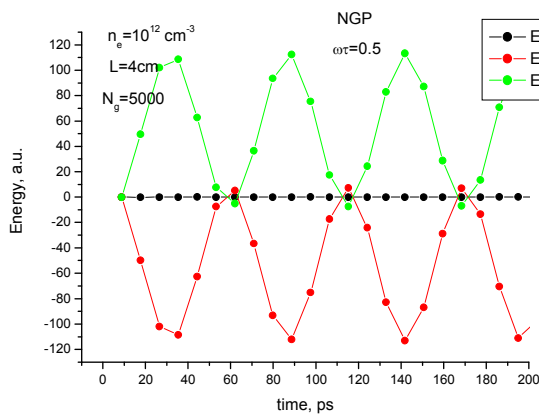
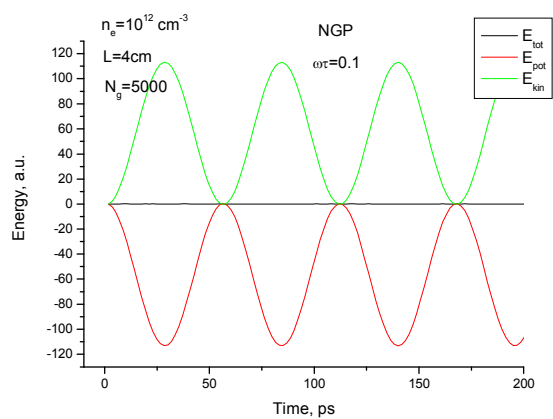
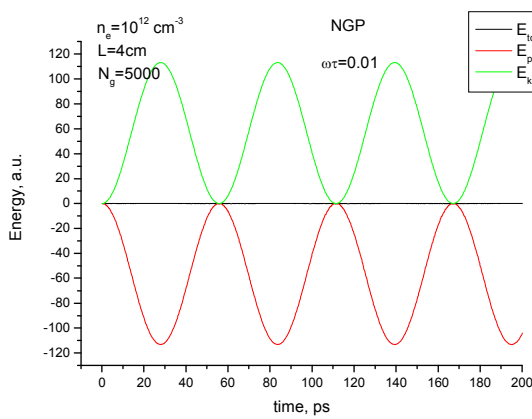
The results of simulation are presented in Fig. 1.



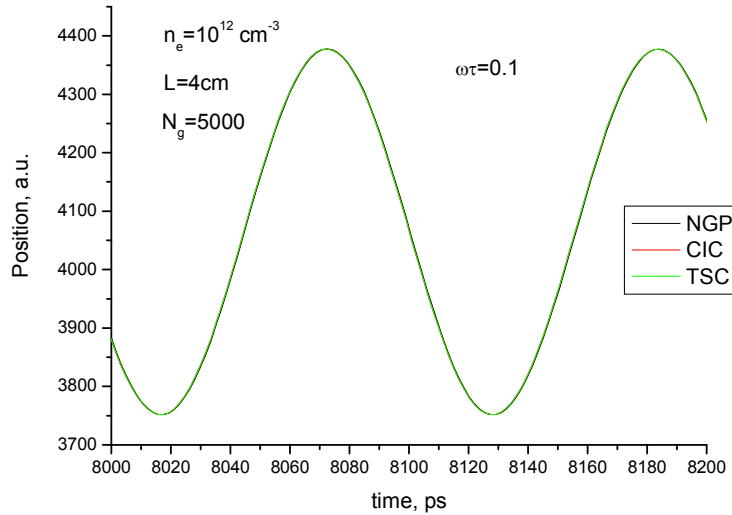
The frequency of plasma oscillation corresponds to calculated value ($\tau=111.4$ ps) and in accordance with theory the amplitude of oscillation conserves unlike its phase:



The energy of oscillations conserves with good accuracy for all values of $\omega\tau$ over a long period of time:



The effect of shape of the weighting function is hardly noticeable for all values of $\omega\tau$. As an example the position of particle for $\omega\tau=0.1$ for three different approximations is shown in Fig. 3:



Comparison of timetables showed that CIC and TSC schemes increased the execution time (as compared with NGP) to only a small extent – about 5%.

The second conventional test is a free drift of charged particles through the matter. The major task of the test is a verification of energy conservation with time because the use of the same weighting functions for charge and force approximations ensures only momentum conservation.

To generate random and uniform initial positions of particles and Maxwellian distribution of their velocities two additional subroutines were included in the code. Typical result for velocity distribution v :

$$v^2 = v_x^2 + v_y^2 + v_z^2$$

of 200000 particles (for $(T/m)^{1/2}=100$) generated by this subroutine is presented in Fig. 4:

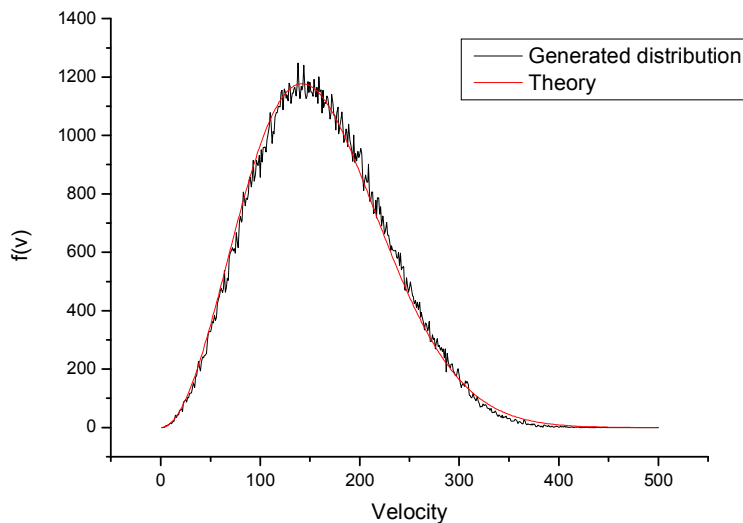


Fig. 4.

A free drift of electrons of low temperature ($v_d=10^9$ cm/s, $T=0.1$ eV) through a neutralizing background of static ions was considered in conditions close to real-life:

$$n_e = 5 \cdot 10^{12} \text{ cm}^{-3}, L = 10 \text{ cm}$$

during a rather long time ~ 100 ns that corresponds to about 10^5 time steps.

Periodical boundary conditions were assumed. The values deduced above for the number of particles and the number of cell were used as a reference point of investigation

$$N_p = 10^5, N_g = 2 \cdot 10^4$$

The influence of a time step on the results of simulation for different weighting functions are presented in Fig. 5 – 7.

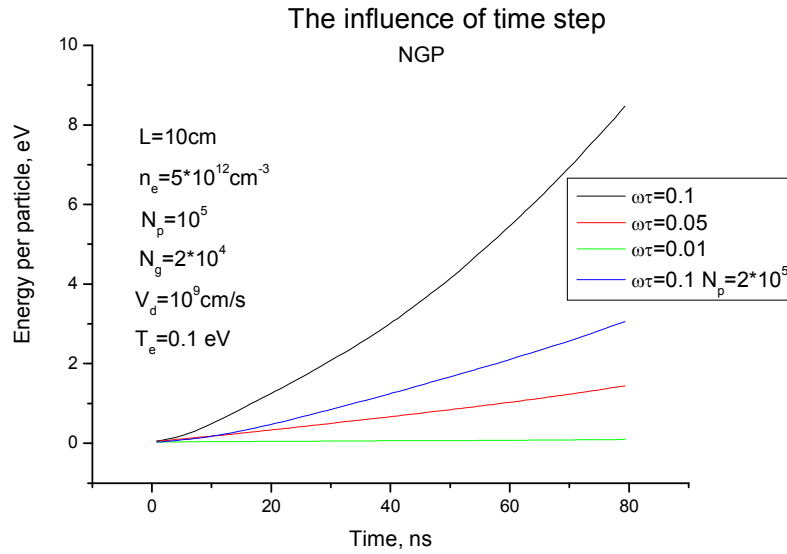


Fig 5.

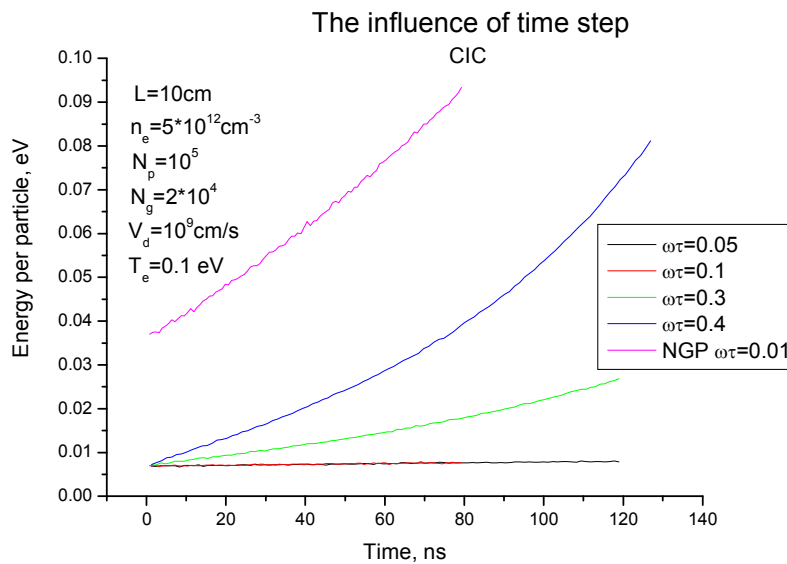


Fig. 6

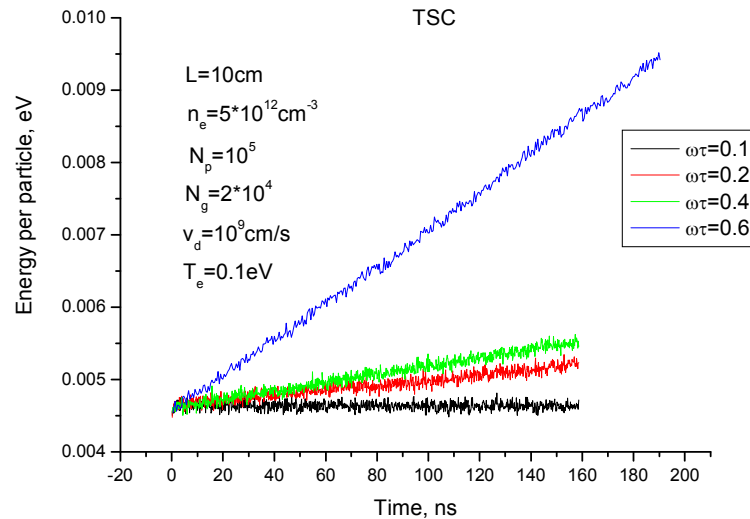
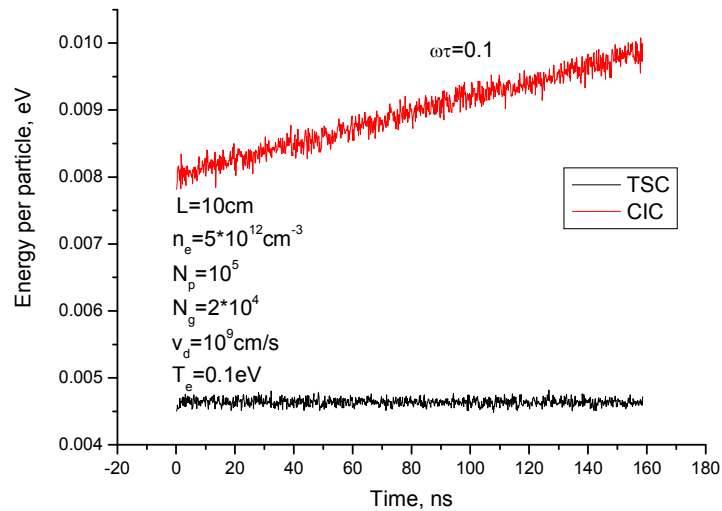


Fig 7.

One can see that NGP approach can be used only when $\omega\tau \leq 0.01$. But even in this case the results are worse than those for CIC with $\omega\tau=0.4$. TSC and CIC schemes give rather close results with a little advantage of TSC.



Dramatically violation of conservation law comes when $\omega\tau \geq 0.8$ in the TSC scheme and $\omega\tau \geq 0.5$ - in CIC (Fig. 8-9).

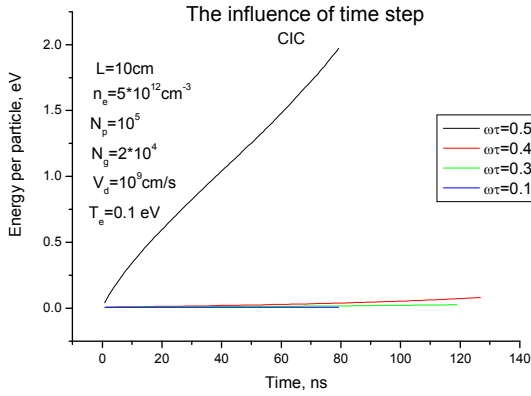


Fig.8

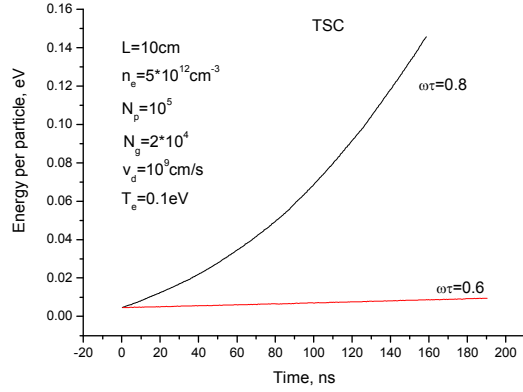


Fig. 9

The effect of node number on the results of simulations is shown in fig. 10-11:

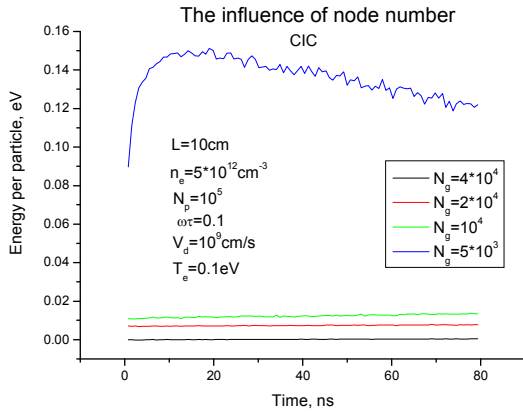


Fig.10

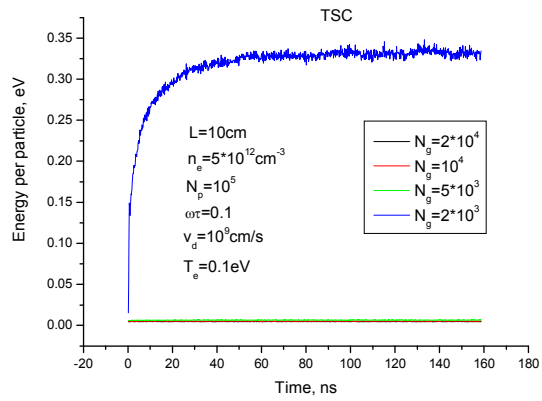


Fig.11

We observe here a similar behavior: the calculations remain appropriate while $N_g > 5 \cdot 10^4$ for CIC and $N_g > 2 \cdot 10^4$ for TSC.

The effect of the number of particle in the problem for the most part comes to an increase in statistical straggling:

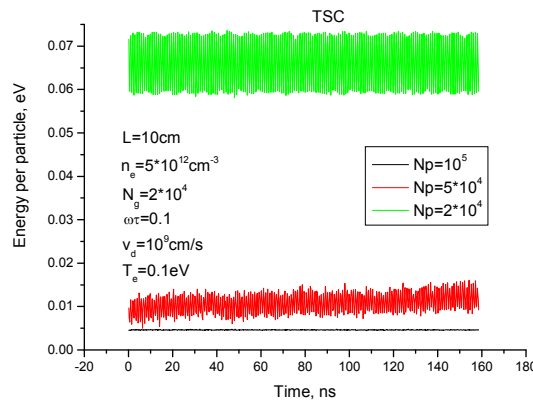


Fig.12

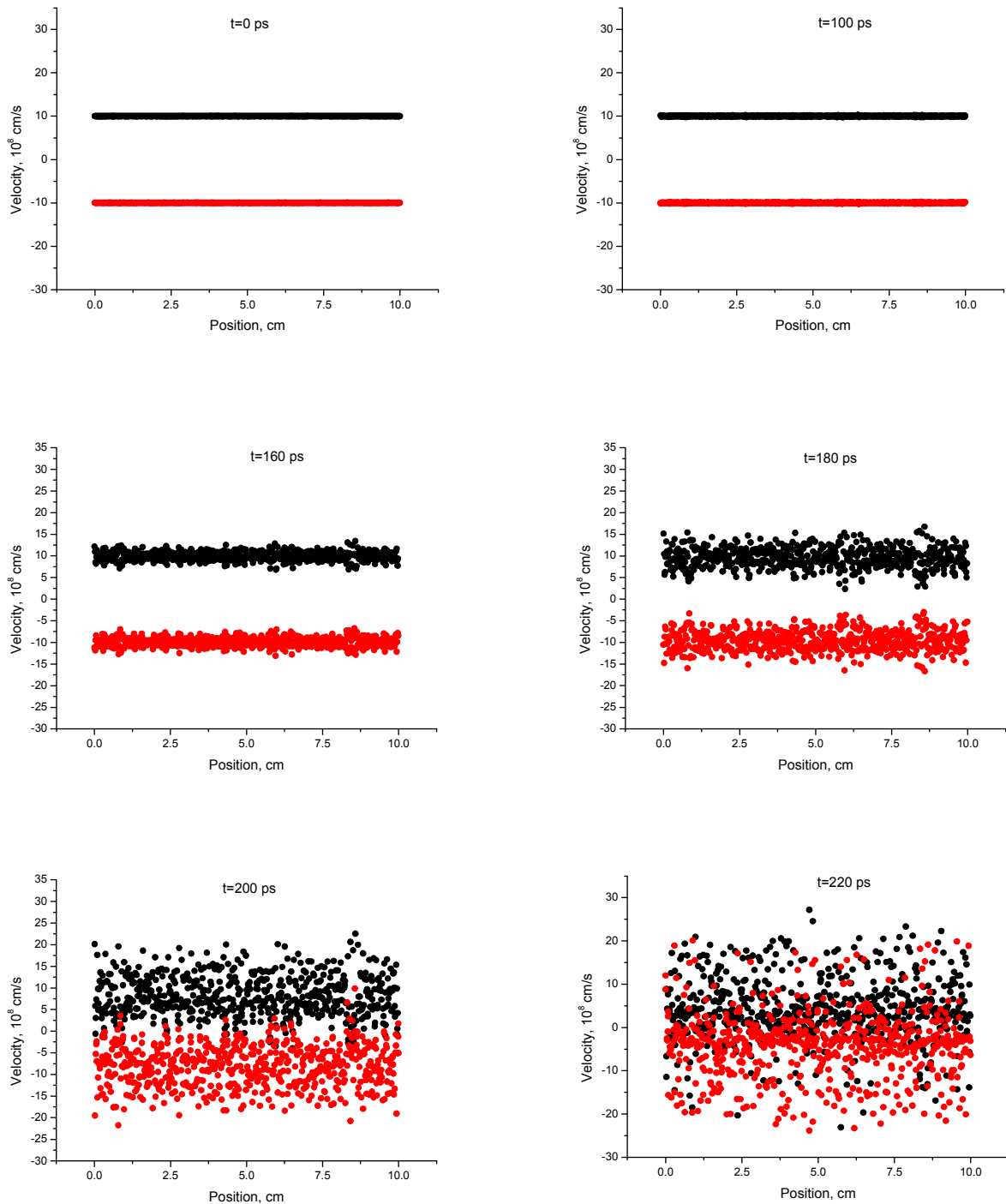
The third conventional test is a simulation of two-stream instability. For the same plasma parameters

$$n_e = 5 \cdot 10^{12} \text{ cm}^{-3}, L = 10 \text{ cm}$$

and two streams of identical particles moving in the opposite directions with velocities

$$v_0 = 10^9 \text{ cm/s}$$

the development of this instability is illustrated in fig. 13:



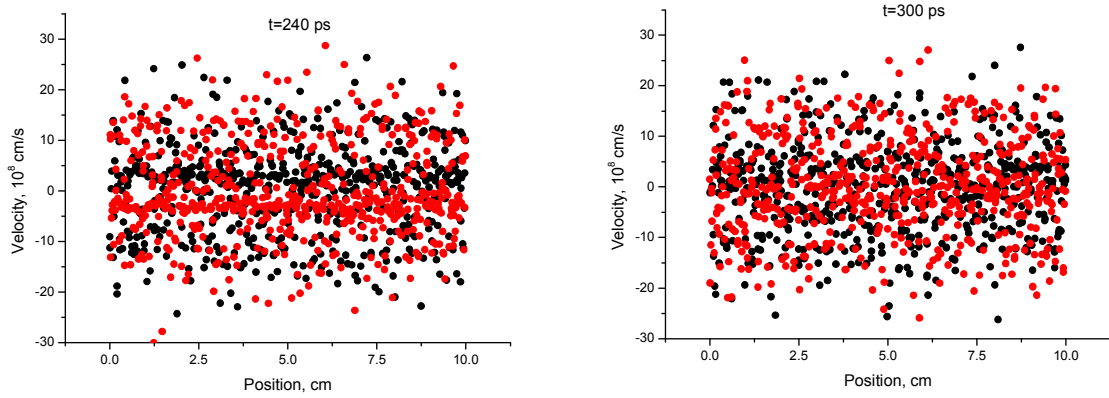


Fig. 13.

The results are rather predictable because the threshold of the development of this instability is defined by the equation [Birdsall]:

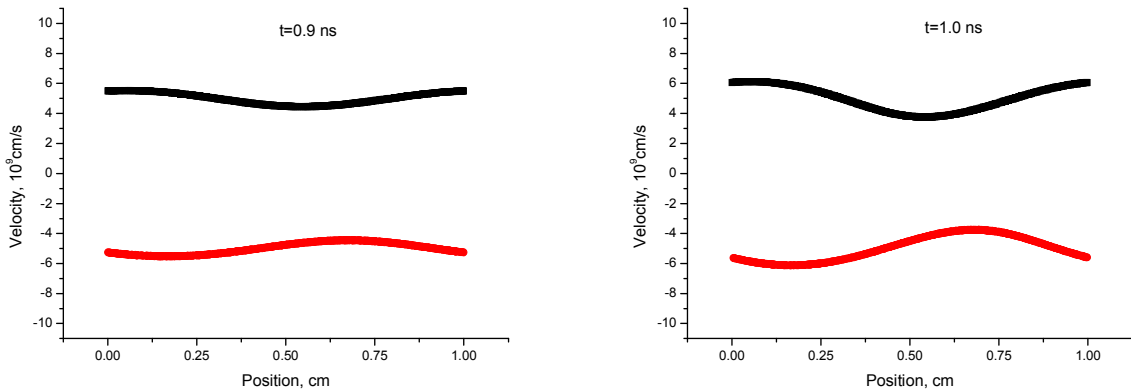
$$\frac{2\pi v_0}{L\omega_p} \leq \sqrt{2}$$

For our conditions ($v_0=10^9$ cm/s, $L=10$ cm, $\omega_p \approx 1.26 \cdot 10^{11}$ s⁻¹) the left side of inequality equals to about $5 \cdot 10^{-3}$ that is very far below the threshold. Much more interesting results should be observed near the threshold. As an example we consider the development of instabilities in plasma with following parameters:

$$n_e = 5 \cdot 10^{11} \text{ cm}^{-3} (\omega_p \approx 4 \cdot 10^{10} \text{ s}^{-1}), L = 1 \text{ cm}$$

To make sure that the instability does not developed when the above inequality is slightly violated we have launched the program at first with drift velocities $v_0=10^{10}$ cm/s ($1.57 > 1.42$). Really, the flows remained stable during some hundreds nanoseconds at least. But when the drift velocities equal to $v_0=5 \cdot 10^9$ cm/s we fall in a region where the increment of growth of instability has a maximum:

$$\frac{2\pi v_0}{L\omega_p} = \frac{\sqrt{3}}{2}$$



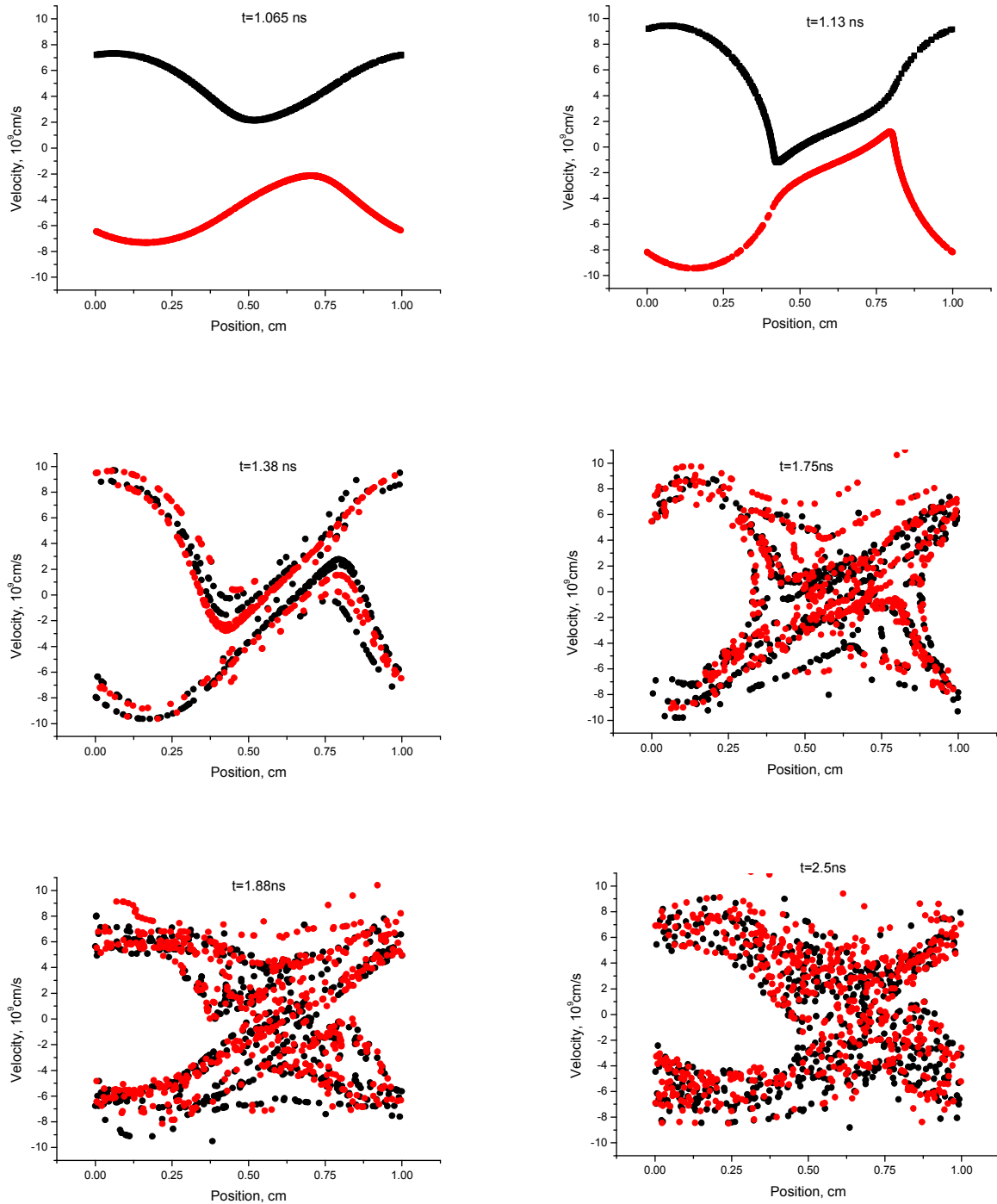


Fig. 14.

Violation of space distribution of charge density and electric potential is illustrated in fig. 15 and fig.16 respectively:

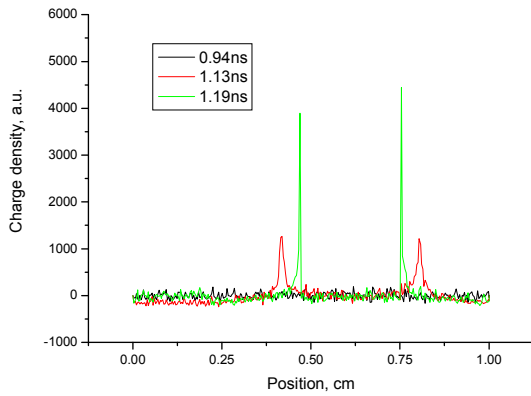


Fig 15.

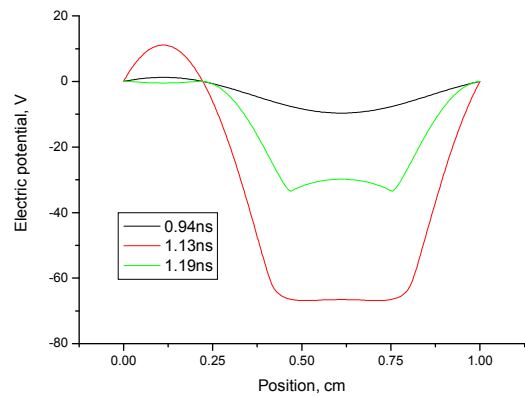


Fig. 16

In order to check the code running under more natural nonperiodic boundary conditions we decided to simulate a vacuum diode to compare its current with Child-Langmuir law. We consider that a cathode is placed on the right at $x=L$ under zero potential. An anode is placed on the left at $x=0$ under potential V . Each time step in the right boundary cell a certain number of macro particles with a temperature of the diode filament are born. This number is defined by the emission current of the diode and by the number of electrons that are simulated by one macro particle. Any electron reaching cathode or anode is considered as dead. These electrons are counted to calculate the cathode and anode current.

The dependence of anode current density on emission current for $L=10$ cm, $V=1$ kV and $T_{em}=0.1$ eV is presented in fig. 17. $N_g=1000$, $\omega\tau=5$ and TSC scheme were used in the simulation. The mean number of particles N_p was about 10^5 that corresponded to 10^4 electrons per macro particle.

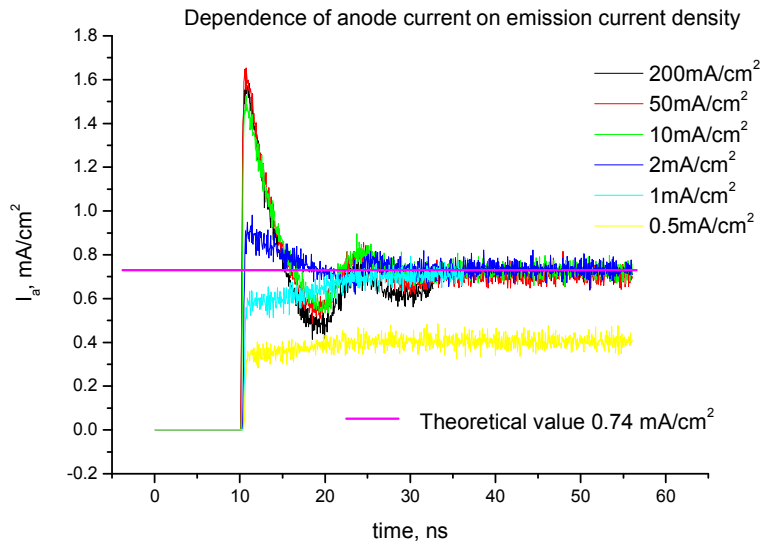


Fig. 17.

The calculations proved to be of little sensitive to modeling parameters and to the shape of weighting function (see Fig 18 - Fig. 22):

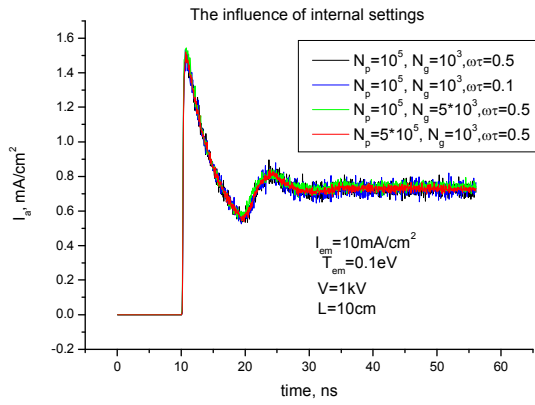


Fig. 18.

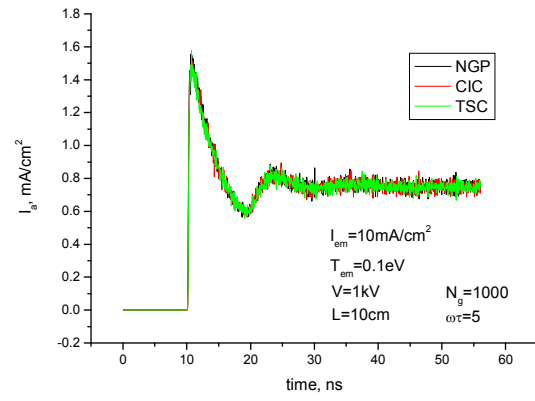


Fig. 19.

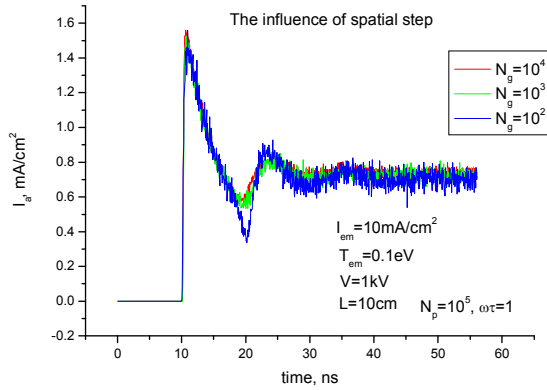


Fig. 20.

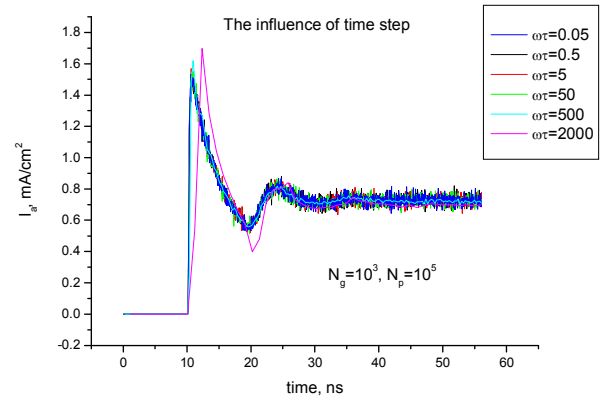


Fig. 21.

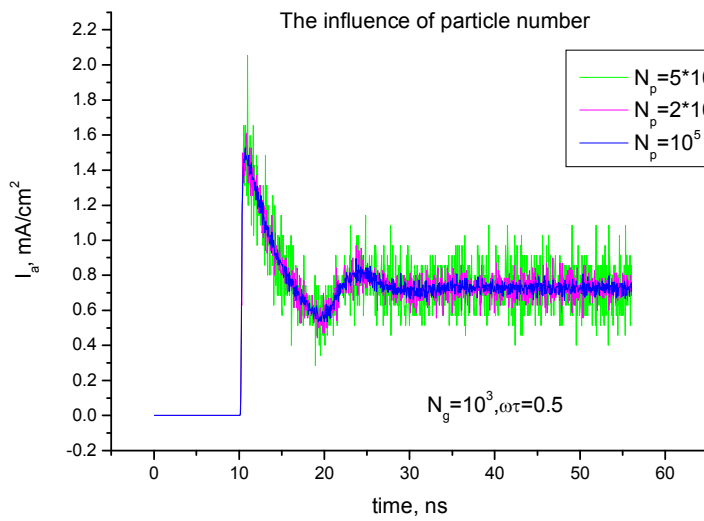


Fig. 22

In this case ω is a relative number: $\omega\tau=1$ corresponds to 2.6ps.

In the conclusion, Fig. 23 and Fig. 24 represent the calculated dependences of the anode current restricted by space charge on diode voltage and electrode spacing. The electric potential distribution in the diode is shown in Fig.25.

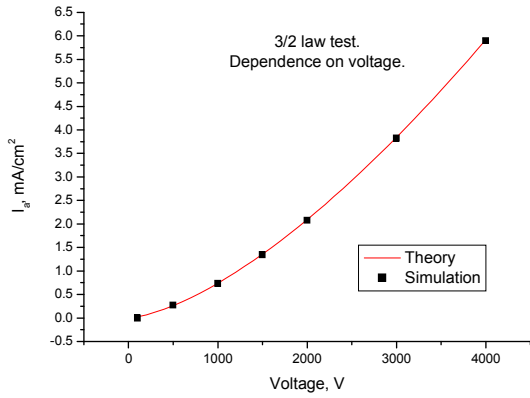


Fig. 23

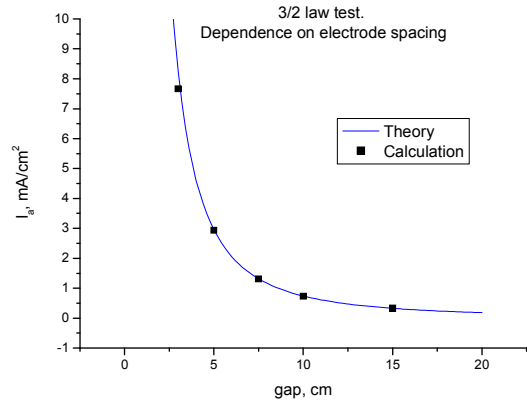


Fig. 24.

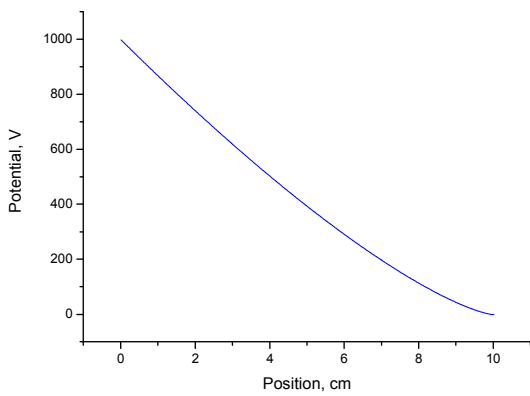


Fig. 25

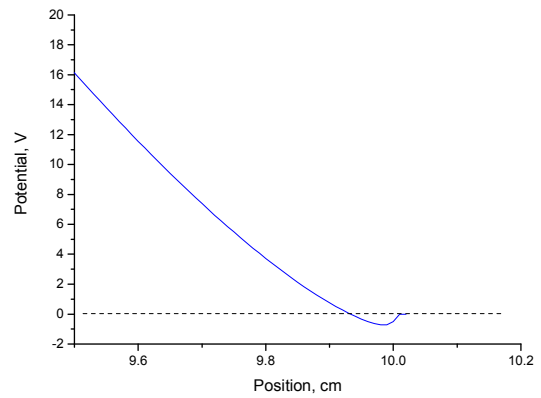


Fig. 25 (detailed).

1D PIC code with Monte-Carlo collisions

Collision or scattering processes can be incorporated in a PIC code by different ways. Because of the wide parameter spread of ECR plasmas are to be considered we will study two of them which are the most widely used now. The first procedure [Hockney] can be more appropriate for the description of dense plasmas with high scattering rates. Another approach [Birdsall] developed for low pressure low density plasmas ($n_e < 10^{10} \text{ cm}^{-3}$, $T_e \approx \text{few eV}$)

The approach of [Hockney] (hereafter – H-scheme) consists in modifying normal mesh time stepping Δt : several free flights are assumed per one field-adjusting time step. So that the previous computing sequence (rotated 180 degree for the convenience) is modified as follows:

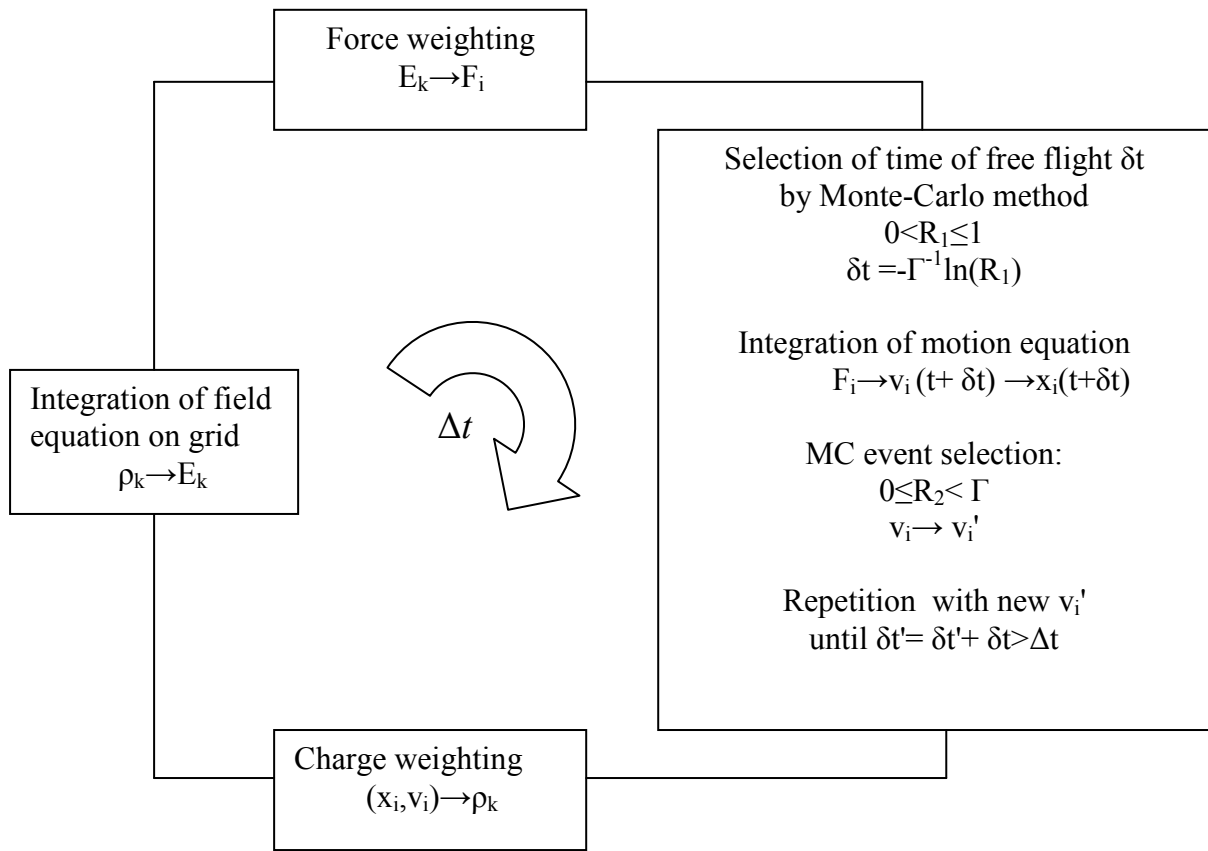


Fig. 26

Here R_1, R_2 – random numbers with the uniform distribution in $(0,1)$; $\Gamma = \sum_{i=1}^p \lambda_i + \lambda_{p+1}$, where λ_i is a probability of i -th scattering; λ_{p+1} (a probability of a dummy self-scattering) is added to make a total scattering rate Γ to be independent of velocity. Here and after when choosing a random continuous value ξ we use the theorem:

If a value of ξ is distributed in the interval (a,b) with the probability density $p(x)$ then the values of ξ can be found from the equation:

$$\int_a^\xi p(x)dx = \gamma$$

where γ is a random number with the uniform distribution in the interval $(0,1)$.

We choose a scattering process comparing R_2 with $\sum_{i=1}^m \lambda_i / \Gamma$ for $m=1..p$. A scattering process will determine a new velocity of the particle v_i' and velocities of new particles if ionization occurs.

The rest of free flight time $\delta t' - \Delta t$ stores in memory to be used on the next field-adjusting time step.

The method described by [Birdsall] (hereafter – B-scheme) is to use only field-adjusting time step Δt . If we know all of collision frequencies and accordingly the total frequency for m -th electron:

$$v_{total} = \sum_i n_i \sigma_i(E_m) v_m$$

the probability of collision of the m -th electron in a time step Δt :

$$P_m = 1 - \exp(-v_{total} \Delta t)$$

(Here we consider that relative electron-ion velocity equals to electron one: $v_m - v_i \approx v_m$.)

The next step is to compare P_m with R_1 . For $P_m > R_1$ the particle m is to be scattered. Which scattering process occurs can be determined by the same way like in previous approach comparing R_2 with v_1/v_{total} , $(v_1+v_2)/v_{total}$, $(v_1+v_2+v_3)/v_{total}$ and so on.

Schematically the computing sequence can be represent by diagram:

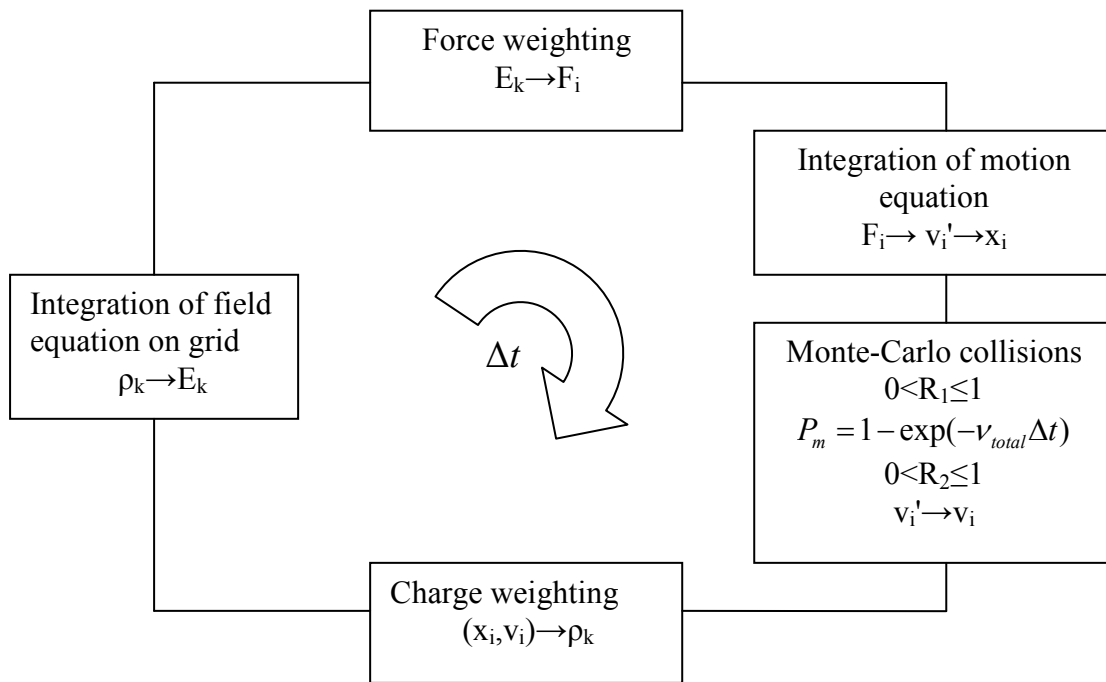


Fig. 27.

To test an operation both of the MCC blocks it was decided to simulate at first an establishment of coronal equilibrium in hydrogen plasma in isothermal D0 approach. In this case only negative ions, neutrals, positive ions and electrons are assumed to be in plasma and for two-particle processes are taken into account: radiative attachment, radiative

recombination, collision ionization and collision detachment. As a check standard the data obtained by the decision of the equation set of recombination-ionization kinetics:

$$\frac{dN_i}{dt} = K_{i-1}N_{i-1} - (K_i + R_i)N_i + R_{i+1}N_{i+1}, \quad \text{for } i=-1, 0, 1$$

(applying implicit scheme and standard procedure for tridiagonal matrix) was used. Here N_i is the number of ions in i -th state; K_i and R_i are the respective ionization and recombination rates. The energies of all electrons are assumed to be identical and equal to 1.35eV. Two different initial conditions were considered: neutral gas with 10^{-2} ionization degree and fully ionized plasma. Total gas density in both cases was $5 \cdot 10^{12} \text{ cm}^{-3}$. The establishments of equilibrium under these circumstances are presented in fig. 28:

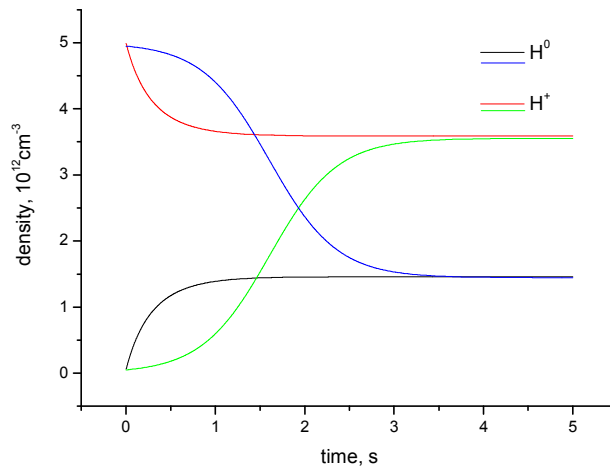


Fig. 28.

The results of comparison with MCC modeling ($N_p=5 \cdot 10^4$) are shown in the figures below. For a small time step ($\Delta t \leq 1 \text{ ms}$) all results are identical:

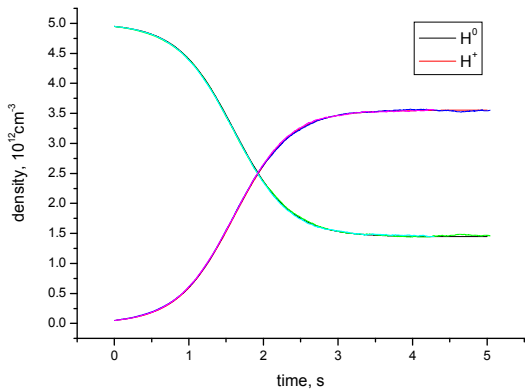


Fig. 29.

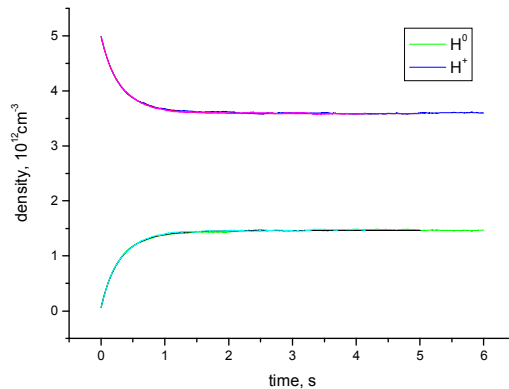


Fig. 30.

Some distinction can be observed only by magnification:

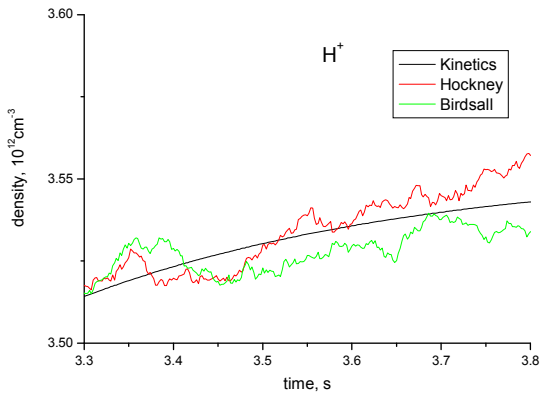


Fig. 31.

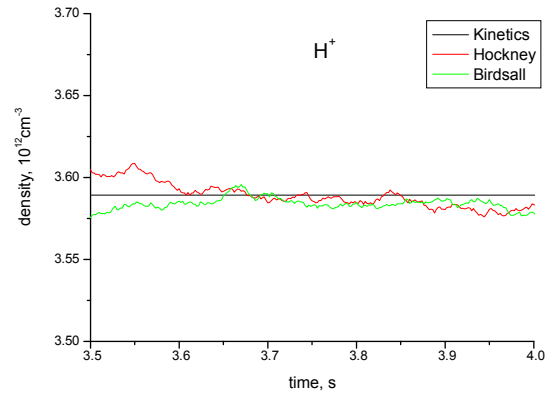


Fig. 32.

Calculation results remain acceptable even the number of particles decreases to 100 (when only one macro electron is present at initial time).

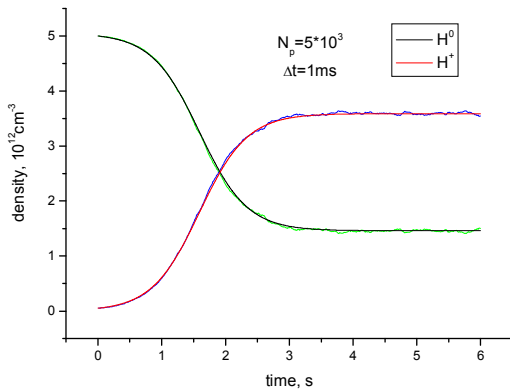


Fig. 33.

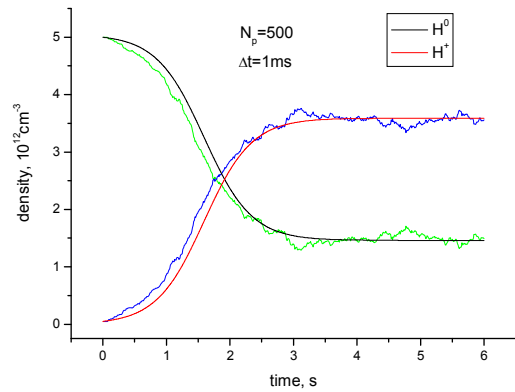


Fig. 34.

At that, both schemes give very close results having similar time consumption (when $\Gamma=1$ is used in H-scheme):

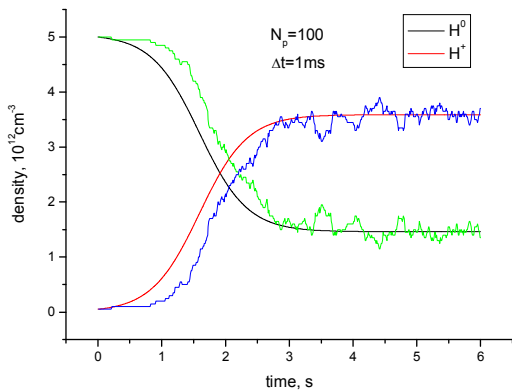


Fig. 35 H-Scheme

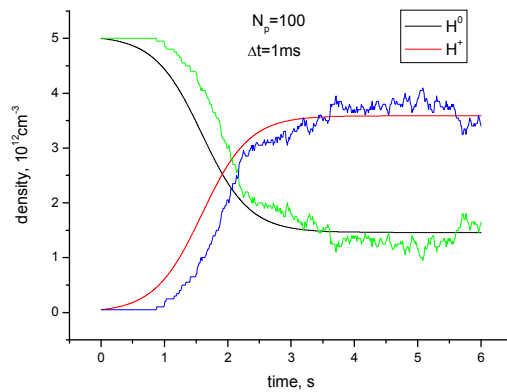


Fig. 36 B-Scheme

It should be noted that a decrease in time step does not improve the results of calculation in this case. Whereas an increase in time step, even though the number of particles to be large, results in a loss of accuracy of calculations.

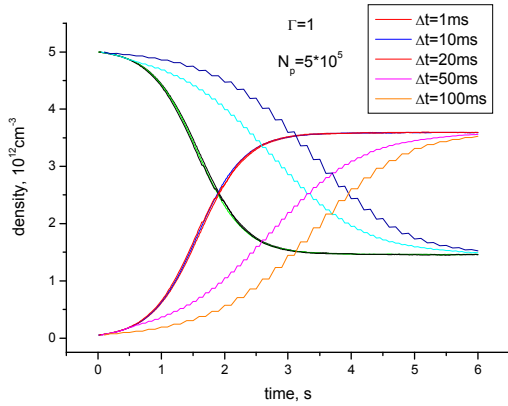


Fig. 37. H-Scheme

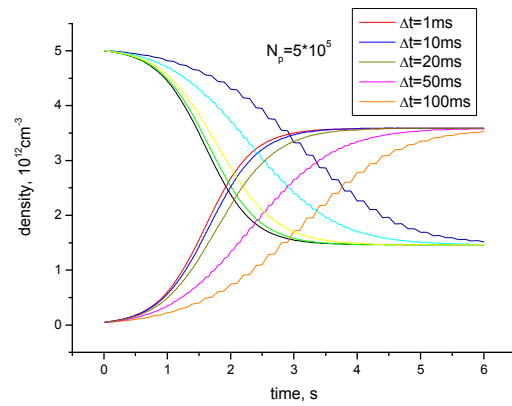


Fig. 38. B-Scheme

The similar picture is observed for the establishment of equilibrium from fully ionized state.

Taking into account that 10ms corresponds to the probability of interactions 0.02, from the figures above it follows that both schemes will give firm results when the total probability of scattering ≤ 0.01 . The scheme, proposed by Hockney, is somewhat more precisely giving a good accuracy up to 0.05. Moreover, this scheme is more flexible. Choosing a proper value for probability of self-scattering (practically – value of Γ) one can change an effective time step only for MCC not touching upon principal mesh timing. The Fig. 39 presents operating of this technique. The precision of calculation improves while Γ increases from 1 to 10. Unfortunately following increase of Γ does not affect on calculation. The reason of this effect is not understood yet.

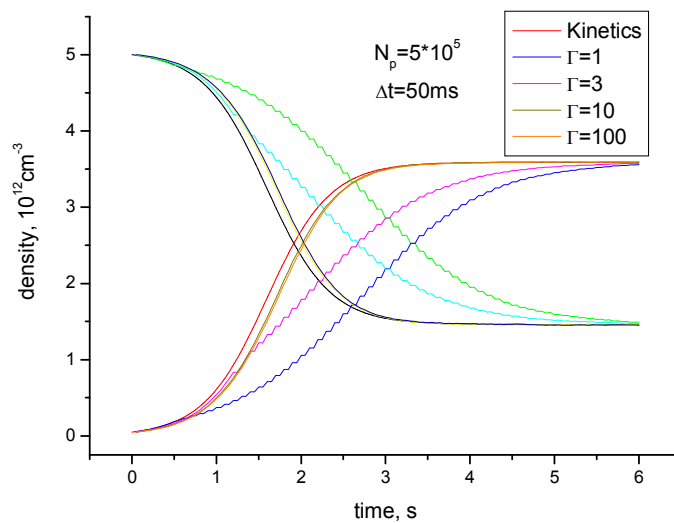


Fig. 39

The technique with variable Γ can be used in opposite manner as well. The results of calculation with $\Gamma < 1$ are shown in fig. 40.

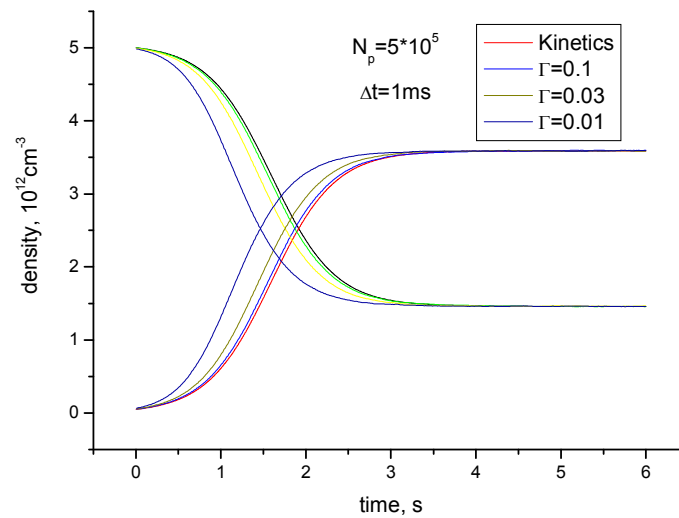


Fig. 40.

In this case the substitution of $\Gamma=1$ for $\Gamma=0.1$ makes the consumption of computational time about 5 times less without any sacrifice of accuracy. But following decrease in Γ is no longer acceptable. This behavior is accounted by the fact that the total probability of scattering for the time step of 1ms equals to $2 \cdot 10^{-3}$. And the effective probability for $\Gamma=0.03$ already exceeds $5 \cdot 10^{-2}$. In any case such feature of the H-scheme allowing to change an effective time step of MCC block (even though in a constraint range) could proved to be very useful.

The observed limitation on a time step should be kept in mind during simulation. In a real problem the restriction on a time step can be even stronger due to an abrupt dependence of collision cross-sections on temperature. An immediate reason of such hard limit on a time step consists in the fact that in essence both of the MC schemes are explicit ones with inherent shortcomings. In case of B-scheme it superposes with additional computational errors caused by substitution $e^x \rightarrow (1+x)$ and $\ln(1+x) \rightarrow x$ that was implicitly assumed during derivation.

1D2V PIC-MCC code

The most appropriate object for testing of joint operating of PIC and MCC blocks of the code is a low pressure plasma discharge. For the most part the electrodes of such devices are lengthy in two directions. So the 1D model is just in place for them to simulate by the code under development. Since a directed particle's velocity in arising drift motion can be several orders less than its mean velocity, at least two components of the velocity has to be taken into consideration in order to calculate the probability of collisions. And in the first approximation we will not go beyond this approach. Unfortunately such approach enables us to consider the all particle's collisions only as hard sphere collisions (the cross-section does not depend on scattering angle and the center of mass scattering angle is uniformly distributed in space). It is rather adequate assumption for collisions with neutral atoms (both electrons and ions) but it is not the case for Coulomb collisions. To avoid ambiguity concerning the problem, for the present we will consider a direct current glow discharge. The ionization degree in the discharge of this kind does not exceed 10^{-5} (typical value is 10^{-7} - 10^{-8}) so that the Coulomb collisions can be neglected with good reason.

So we will describe the velocity of charged particles by two quantities: the longitudinal velocity v_x and the square of the component of the velocity lying in the plane perpendicular to the x direction: v_{\perp}^2 . The probabilities of particle's collisions will be defined using the total velocity of the particle:

$$v_{tot} = \sqrt{v_x^2 + v_{\perp}^2}$$

Keeping in mind the main goal, a glow discharge in hydrogen was chosen as an object for simulation. The following nine processes having the largest cross-sections were taken into consideration for electron-neutral collisions:

- elastic scattering;
- rotational excitation;
- vibrational excitation;
- electronic excitation of $b^3\Sigma_u^+$ state;
- electronic excitation of $B^1\Sigma_u^+$ state;
- electronic excitation of $C^1\Pi_u$ state;
- electronic excitation of $B'^1\Sigma_u^+$ state;
- electronic excitation of $E^1\Sigma_g^+$ state;
- ionization.

For ion-neutral collisions only elastic collisions were accounted for because of relatively small cross-sections of ionization and excitation. The effect on the neutral gas is not calculated.

To shorten consumption time a 2D table of collision frequencies is generated in the beginning of simulation. The m -th column of the table represents the sum of respective frequencies $\sum_{i=1}^m v_i$ for different quantities of particle's velocities which squares are placed in 0-th column. The retrieval of necessary value is performed by binary search during the run-time. The cross-sections of the processes were taken from [Tawara]. The decision as to what kind of collisions has occurred is taken in the way described in the previous section.

The scattering angle and new velocity (or velocities in case of ionization) of the particle are determined in the following way.

For elastic collisions of electrons with background molecules ($m_e \ll M$) the energy of scattered electron is defined by equation:

$$E_{scat} = E_{inc} \left(1 - \frac{2m_e}{M} (1 - \cos \Theta) \right)$$

where E_{inc} is the incident energy and Θ is the scattering angle. (We do not neglect the small quantity of energy loss to describe correctly the electron drift while the energy of electrons is below the threshold of neutral excitation.) In hard sphere approximation the velocity of the electron after collision is considered to be uniform. Therefore the new longitudinal velocity is

$$v'_x = v'_{tot} \cos \Theta$$

where $\cos \Theta$ is uniform in the interval (-1,1) and can be obtained from relation:

$$\cos \Theta = 1 - 2R$$

Hereafter R is a uniform random number in the interval (0,1).

The term v'_{tot} is the new total velocity corresponding to the new electron energy E_{scat} .

Another component of the velocity is

$$v_{\perp}^2 = v_{tot}^2 - v_x^2$$

We will use also the same approximation for inelastic electron-neutral collisions with the only difference that the energy of scattered electron in case of excitation collisions will be defined by equation:

$$E_{scat} = E_{inc} - E_{excit}$$

where E_{excit} is the excitation energy. And for ionization collisions this energy is

$$E_{scat} = E_{inc} - E_{ion} - E_{creat}$$

Here E_{ion} is the ionization energy. We neglect here the small energies of the neutral and the created ion. In addition we consider that the overwhelming contribution into the total ionization cross-section is made by collisions in which the transferred energy is small and respectively the energy of created electron E_{creat} is small too. Therefore E_{creat} is regarded as a free parameter with typical value ~ 0.1 eV. The velocity of the created electron is considered to be uniform.

For elastic scattering of ions in hard sphere approximation we have

$$E_{scat} = E_{inc} \cos^2 \chi$$

where $2\chi = \Theta$ is the center of mass scattering angle. Respectively

$$v'_x = v'_{tot} \cos \chi$$

where

$$\cos \chi = \sqrt{1 - R}$$

We have chosen for simulation a discharge in a tube 20 cm long filled with hydrogen under the pressure of 0.2 torr. To initiate the discharge we assumed that the cathode can emit electrons with the temperature of filament (~ 0.1 eV) and small current density 10^{-7} A/cm² and the voltage of 1200V is applied between the anode and the cathode. The cathode is made of material with secondary emission coefficient 8.e-3. All these values are typical for DC glow discharges. Since the voltage-current characteristic of the discharge is horizontal in the region of interest, i.e. the current of the discharge can spontaneously rise if the applied voltage is maintained constant turning the discharge into abnormal one and then – into the arc, it is necessary to fix the operating point by simulating an electric circuit. Therefore it was considered that the full voltage was applied to the discharge tube through a resistor. After a few trial runs its resistance was decided to be of 10^7 Ohm·cm².

To get a steady state of the discharge we need to include into consideration a process of charge particle destroying. Depending on discharge conditions it can be a volume recombination (discharge controlled by recombination) or the recombination on the walls of

the discharge tube (discharge controlled by diffusion). In accordance with experimental data in the conditions under consideration it is diffusion that controls the discharge. The frequency of the recombination (diffusion loss) in case besselian density profile is

$$v_{da} = D_a / \Lambda^2 \quad ; \quad \Lambda \approx R / 2.4 ,$$

where D_a is the coefficient of ambipolar diffusion, R – the radius of the discharge tube. We used the table value for D_a and the radius of the tube was varying value. The decision as to which particle suffers a recombination was made by the manner borrowed from [Burger]. We calculated the sum of individual probabilities $P_c = v_{da} \Delta t$ of the particles in accordance with the sequence in which they were recorded. The particle whose probability made this sum larger than 1 suffered the recombination and the summing was restarted with the sum decreased by 1. The sums for ions and electrons were saved from step to step to resume the process on each step from previous values.

Testing of the code was started from the regime of dark discharge: the space charge does not disturb the external electric field. In this case the charged particles drift in the constant electric field. Following an individual particle gave us a possibility to compare the calculation data with the results of analytical solution. The results are shown in figures 41-42.

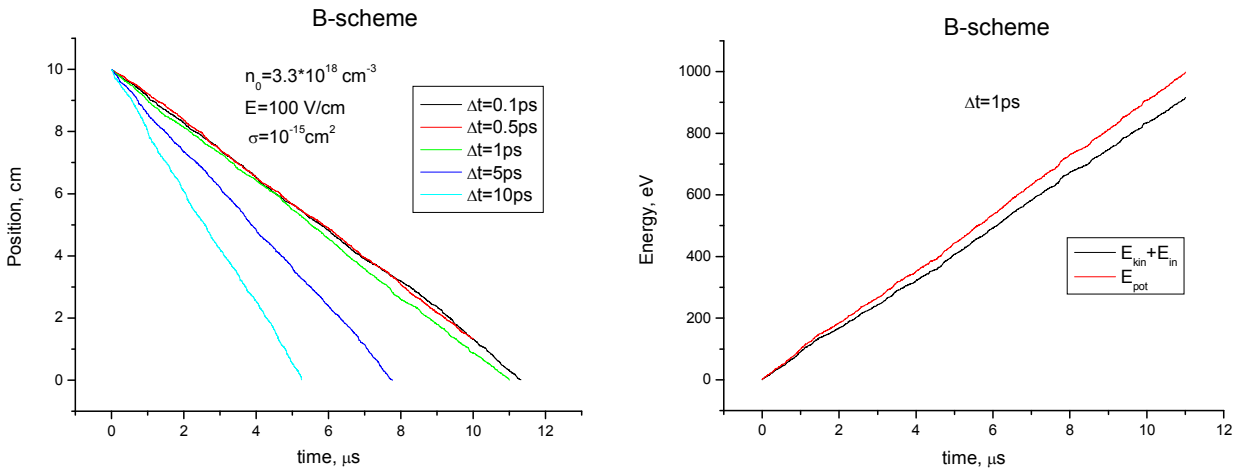


Fig 41. Position of an electron and its energy verses the time.

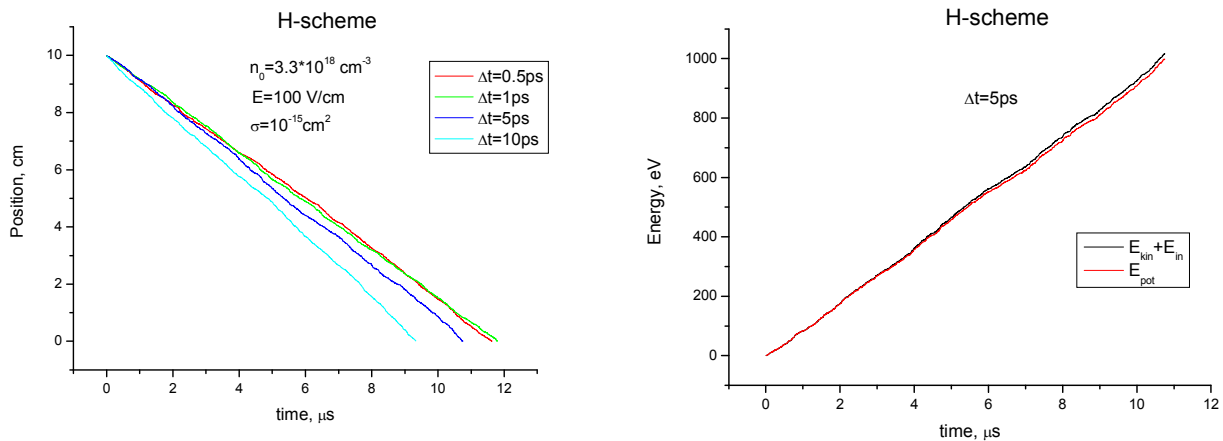


Fig. 42. Position of an electron and its energy verses the time ($\Gamma=1$).

For the convenience of comparison all kinds of collisions except elastic ones were “switched off”, the cross-section $\sigma(v) \equiv \sigma = 10^{-15} \text{ cm}^2$ and the density of neutrals was increased up to 100 torr. As may be seen the drift velocity tends to $0.87 \cdot 10^6 \text{ cm/s}$. At the same time the mean velocity of the electrons is about $5.2 \cdot 10^7 \text{ cm/s}$. It is in a rather good agreement with the results of kinetic theory that give respectively:

$$v_d = \mu_e E = \frac{eE}{m\nu_{tr}} = \frac{eE}{mn_0 \langle v \rangle \sigma_{tr}}$$

$$\langle v \rangle = \sqrt{\frac{2}{\delta}} \frac{eE}{m\nu_{tr}} = \sqrt{\frac{2}{\delta}} v_d$$

Here $\delta = 2m/M$ is the part of energy transferred in one collision; σ_{tr} is the transport cross-section and E – the electric field. In easy to use form

$$v_d \approx \frac{3.52 \cdot 10^7}{\sqrt{n_0 \sigma_{tr}}} \delta^{1/4} \sqrt{E} \quad \text{cm/s}$$

(Here E in V/cm). The substitution by numerical quantities gives $v_d \approx 0.93 \cdot 10^6 \text{ cm/s}$ and $\langle v \rangle = \sqrt{2/\delta} v_d \approx 5.6 \cdot 10^7 \text{ cm/s}$ ($\delta \approx 5.487 \cdot 10^{-4}$). The small discrepancy may be the sequence of different interpretation of mean velocity since the calculated value of the ratio $v_d/\langle v \rangle \approx 1.67 \cdot 10^{-2}$ coincides with $\sqrt{\delta/2} \approx 1.66 \cdot 10^{-2}$ to within 1%. (Running a few steps forward, it should be noted that 1D3V model gives exactly the same results for drift and mean velocities).

In this test the H-scheme gave also the better accuracy compared with the B-scheme. The reasonable accuracy $\sim 5\%$ can be obtained only for the time step $\leq 1 \text{ ps}$ (or $\leq 2 \text{ ps}$ for the H-scheme). Because the frequency of collisions under this circumstances

$$\nu^{-1} = 1/n_0 \sigma_{tr} \langle v \rangle \approx 5.8 \cdot 10^{-12} \text{ s}$$

we have got thereby the requirement on the time step:

$$\nu \Delta t \leq 0.2$$

So in the simulation of glow discharge with the density $n_0 = 6.6 \cdot 10^{15} \text{ cm}^{-3}$ and total collision cross-section $\leq 2 \cdot 10^{-15} \text{ cm}^2$ ($\nu \approx 3 \cdot 10^8 \text{ cm/s}$) we can use with certainty the time step $\Delta t \sim 20 \text{ ps}$. The size of spatial step h can be chosen from the relation:

$$E \cdot h \ll E_{excitation}$$

that gives the number of nodes $N_g \sim 1000$. To ensure a good statistical accuracy the number of particles N_p should be

$$N_p \sim (100 \div 500) \cdot N_g = (1 \div 5) 10^5$$

Since this value is not fixed directly and is defined by the steady current of the discharge that is also unknown in advance some trial runs were required to define the number of electrons and ions in the macro particle N_s . This value equals to $2 \cdot 10^3$ to provide $N_p \approx 3 \cdot 10^5$.

Before demonstration the results of the simulation it would be well to refresh the main properties of DC glow discharge. The particular features are a cathode layer with specific structure and a large quasi neutral region filling the space between the cathode and anode layers – a positive column. The glow pattern is shown in fig 43. The region with maximum glow intensity is the space of Negative Glow. It sharply separated from the cathode dark space and than the intensity of glow smoothly decreases towards the anode changing into the Faraday Dark Space. Next – the glowing Positive Column. Its intensity is smaller than this of the negative glow and sometime has a layer-like structure (stratified). The strata usually move in the direction towards the cathode with typical velocity $10^4 \div 10^6 \text{ cm/s}$. The results of simulation are presented in figures below.

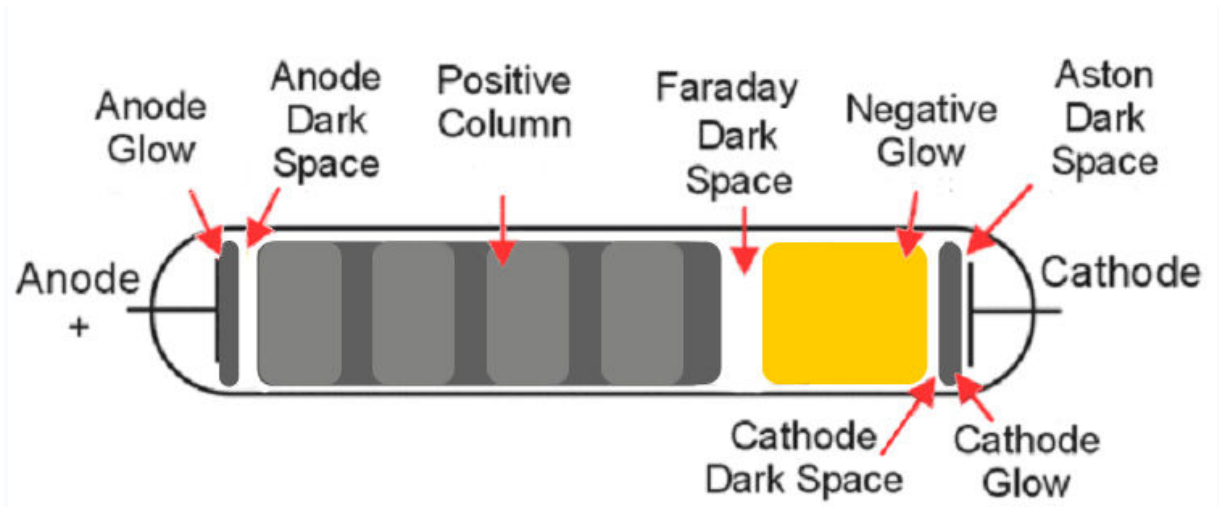


Fig 43. Schematic sketch of DC glow discharge.

The total current discharge is presented in fig 44.

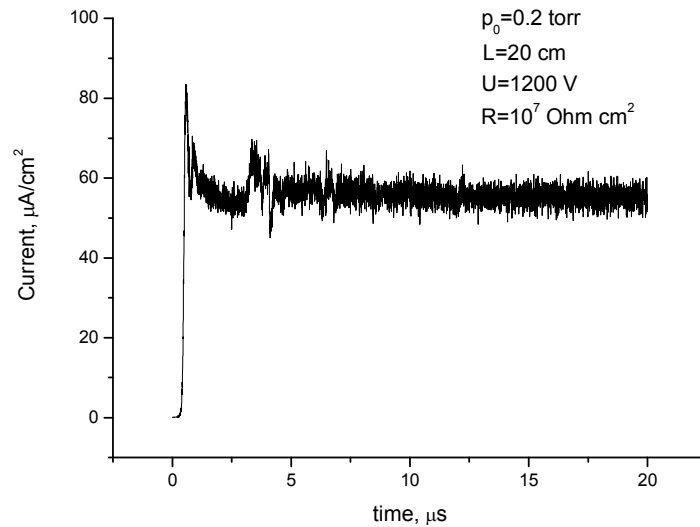


Fig. 44

One can see that after 10 μs the discharge becomes settled with the steady state current density of about $55 \mu\text{A}/\text{cm}^2$. The spatial distribution of total glow usually follows the electron density that is shown in fig 45 (the anode is on the left). In the figure one can see the region of negative glow and the stratified positive column. The strata are not stable as may be seen in the fig. 46. They run towards the cathode with phase velocity of about $2 \cdot 10^6 \text{ cm/s}$. The picture remains similar during the all time of simulation. The formation of the discharge structure is illustrated in fig. 46a-46c.

It is not possible to resolve the Aston and Cathode Dark spaces in the picture but it can be done from the plot of mean electron energy vs the position of electron (Fig 47). Because the Astone dark space is caused by low electron energies (below the threshold of excitation of the respective levels of the molecule; it is of about $\sim 10\text{eV}$ in our case) and the cathode dark space is due to high electron energies (far above the maximum of respective cross-section; it is of about $50\div 70\text{eV}$). So one can consider that the dark spaces is positioned in the interval (19.8, 20) cm and (18.2, 18.5) cm. The bulk space between them is the cathode glow.

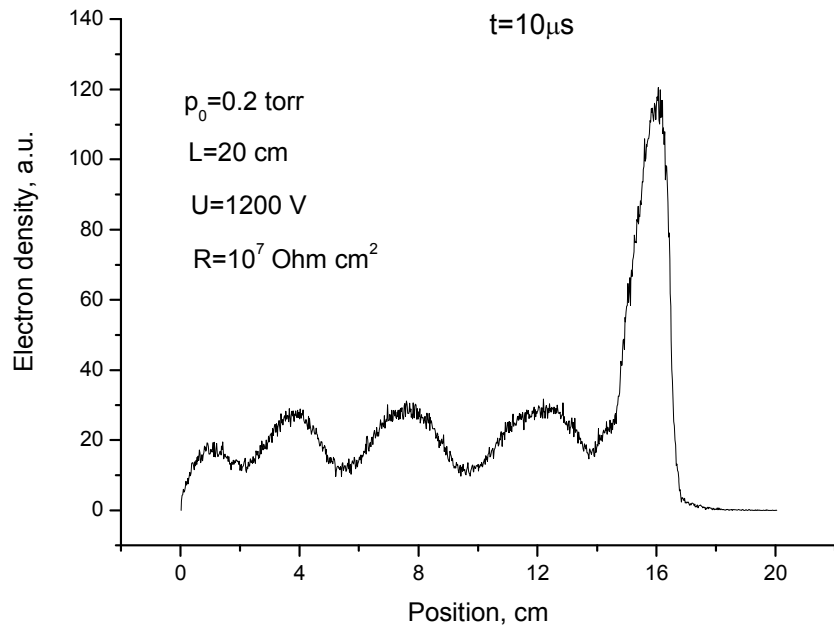


Fig. 45

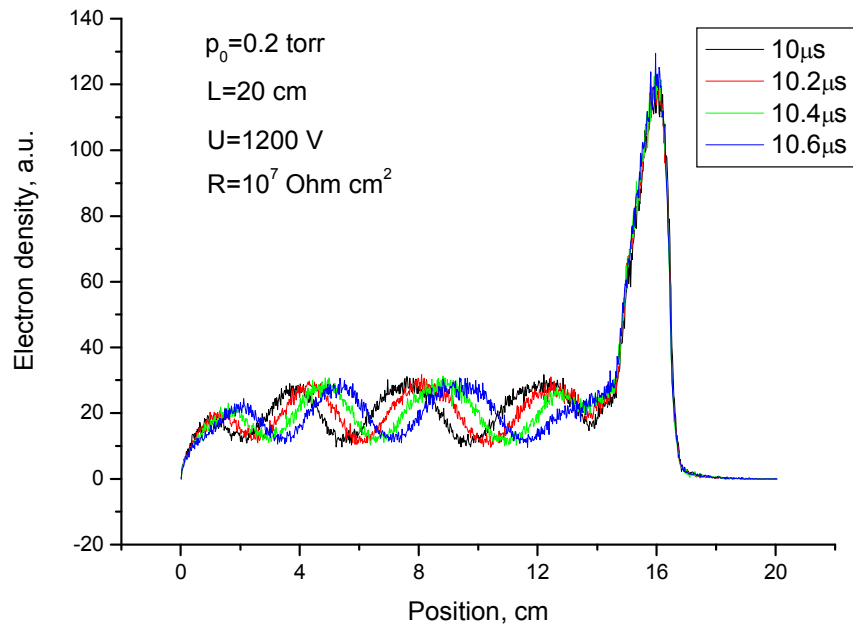


Fig. 46

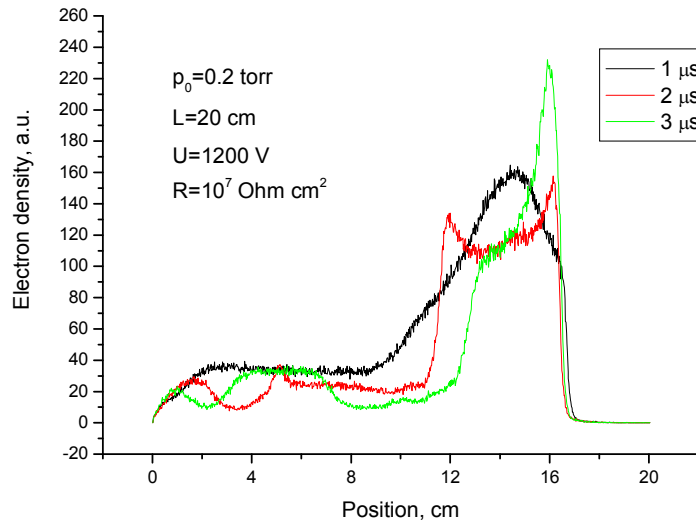


Fig. 46a

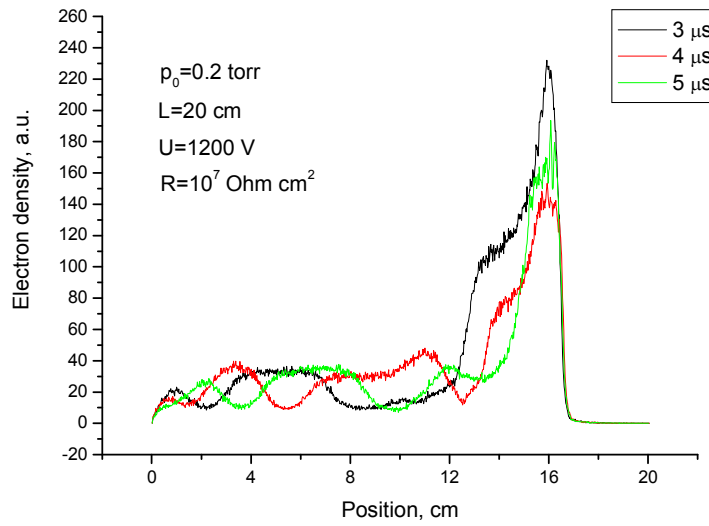


Fig 46b

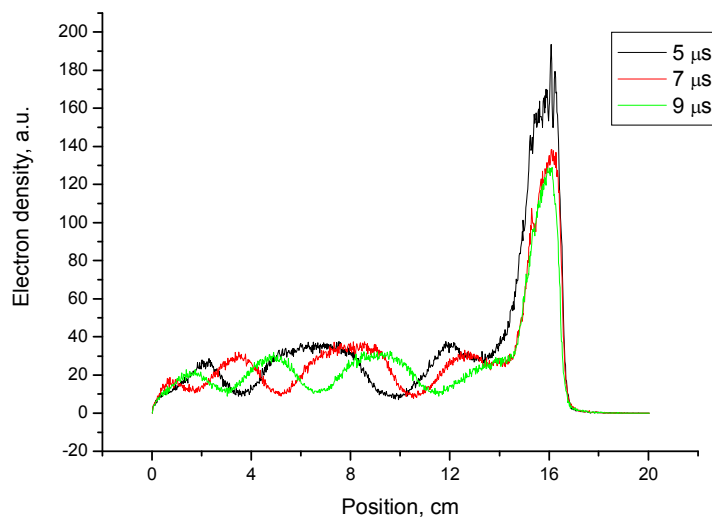


Fig. 46c

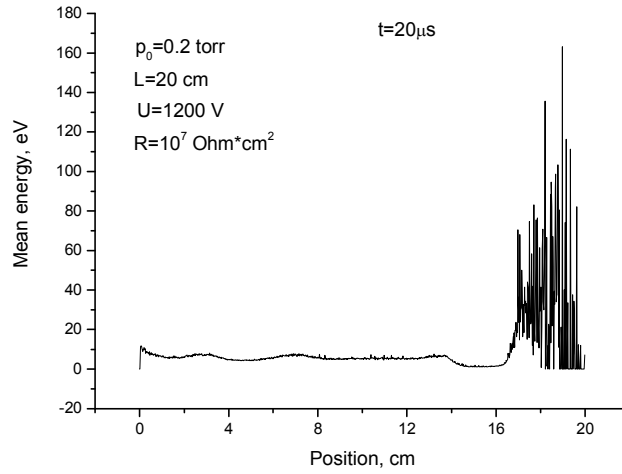


Fig 47. Mean electron energy vs position

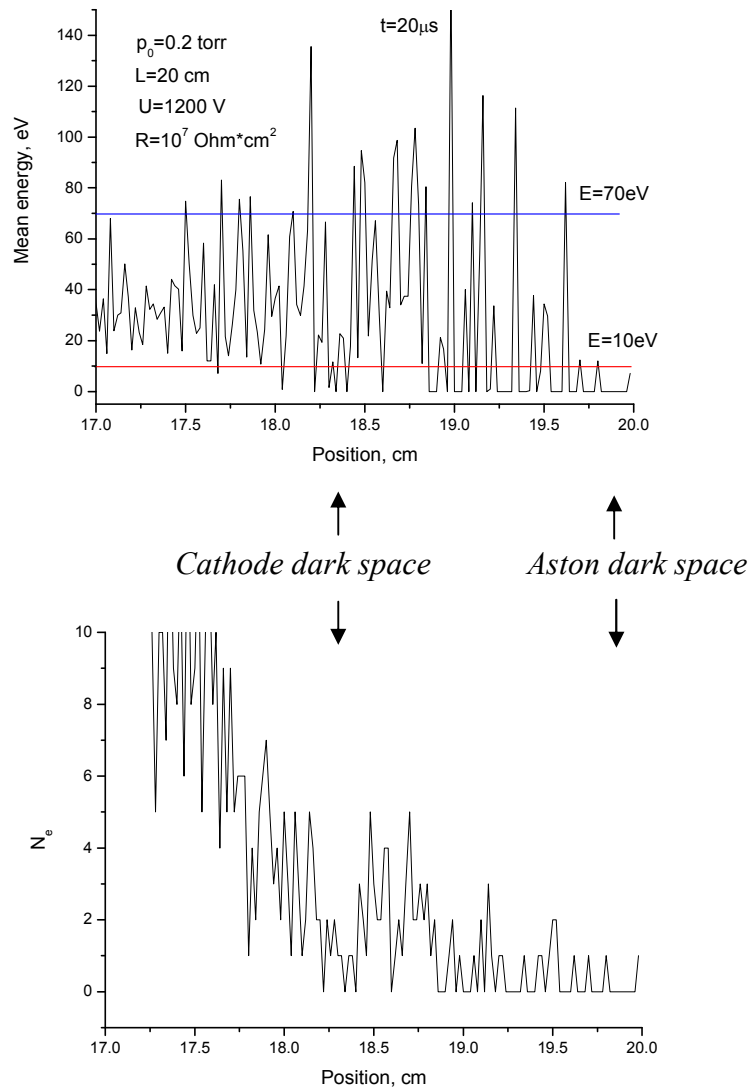


Fig 47a. Mean electron energy and the number of electrons vs position (zoomed in)

The fine structure of the glow on the left side can be seen from Fig 47b. The increase of electron energy near the anode is responsible for the anode glow. The electron energy distribution function all over the glow discharge at $t=20\ \mu\text{s}$ is presented in fig 48.

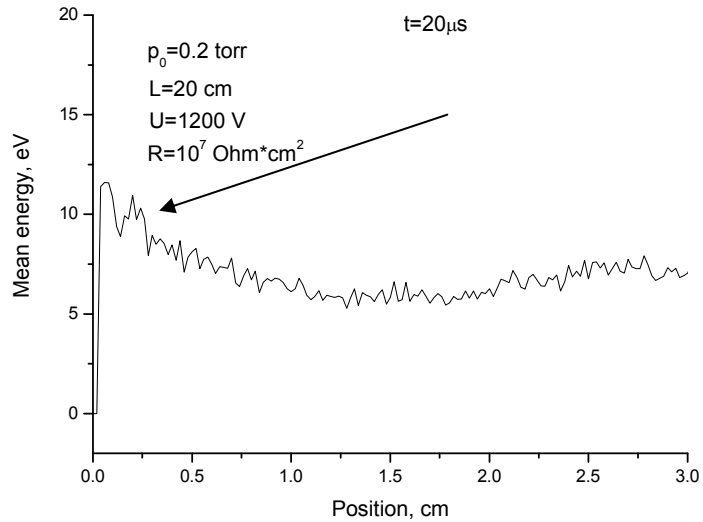


Fig 47b. Mean electron energy vs position (zoomed in)

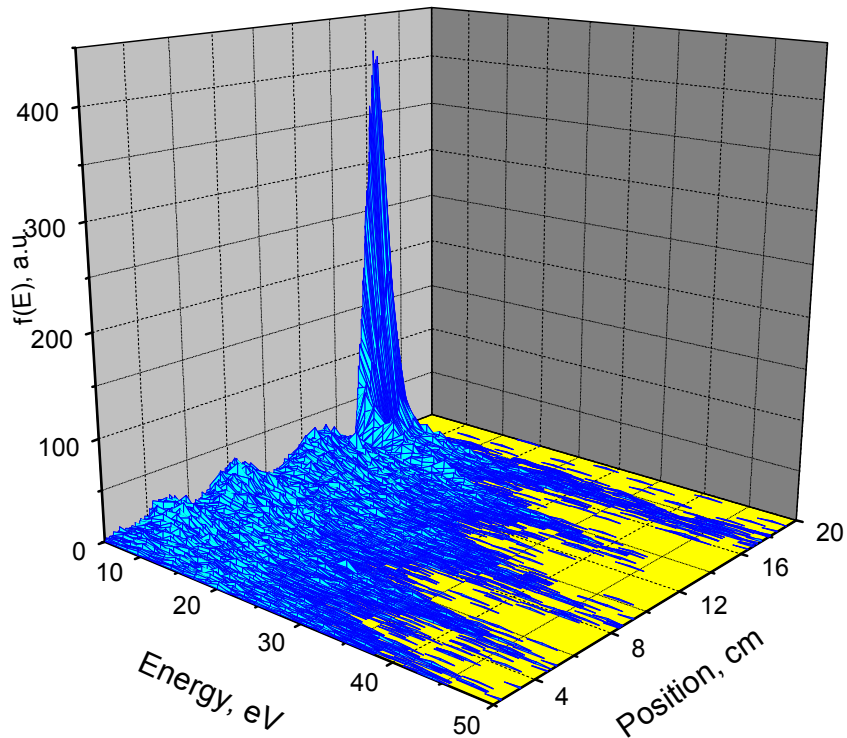


Fig. 48

The spatial distribution of potential, electric field and total charge are presented in figures 49-51 respectively. The figure 52 represents the comparative distribution of electrons and ions in the discharge. These pictures are qualitatively agree with experimental data including the plateau on the voltage distribution in the region of negative glow and the ripple on the electric field distribution in the region of positive column. But there is some quantitative discrepancy in comparison with experimental data. In the regime of normal discharge (the cathode spot occupies the full surface of the cathode) the value of the cathode drop U_c and the thickness of cathode layer d_c are fixed and defined by the gas properties and gas pressure. According to the tabulated experimental data in our conditions they are $U_c \approx 280V$ and $d_c \approx 5cm$. But now we have respectively $U_c \approx 480V$ and $d_c \approx 3.5cm$. Since the values are defined by electron swarm in the cathode layer the discrepancy can be result from inadequate description of ionization processes in our model. Therefore we put off the final establishing the reason of the fact till the comparison with the results of 1D3V model.

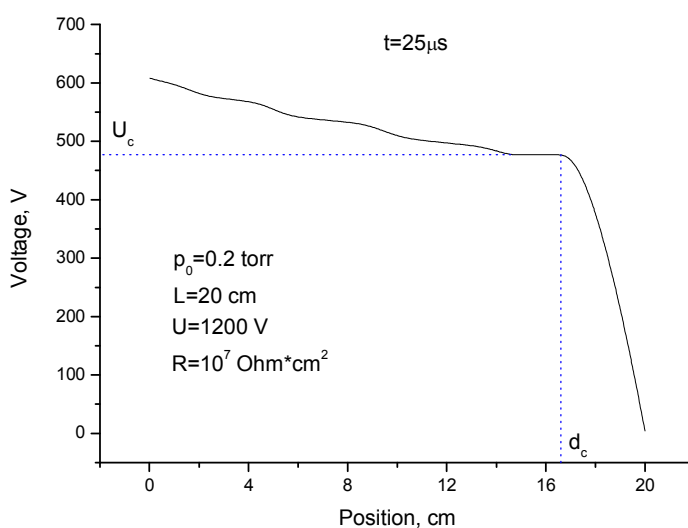


Fig.49

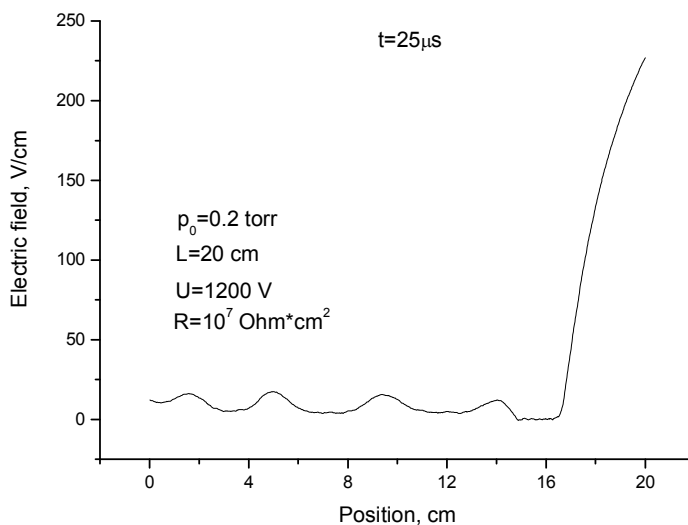


Fig 50

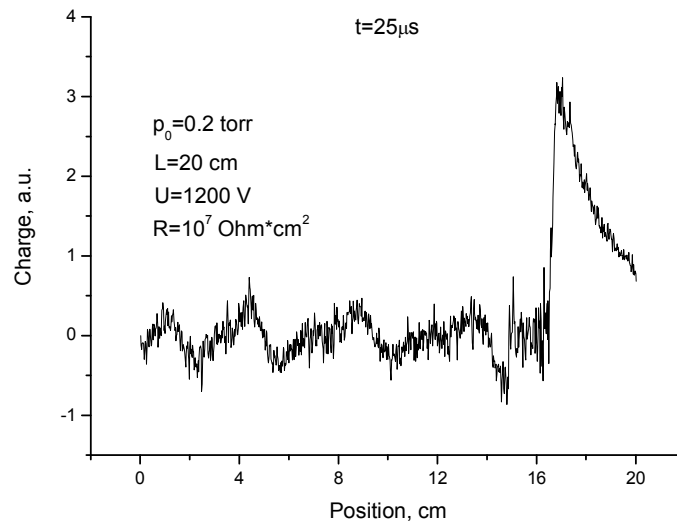


Fig. 51

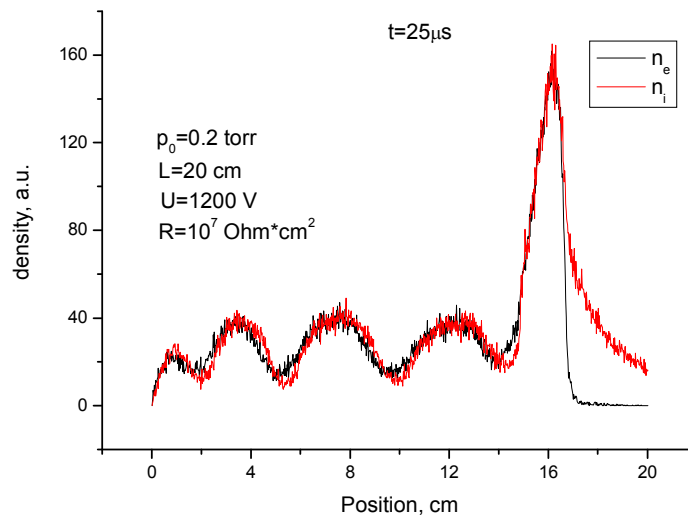


Fig. 52

The influence of the time step on the result of simulation is demonstrated in fig. 53-54. The time consumption for the time steps 20 ps, 50ps, 100 ps and 200 ps were respectively 51h 15min, 22h 16min, 17h 00min and 12h05 min. It should be noted that all attempts to run the program with 500ps and larger time steps were failed. Nonlinear dependence of the consumption time on the number of time steps is accounted for by the increase in the discharge current and respective increase in the number of macro particle with the increase in time step.

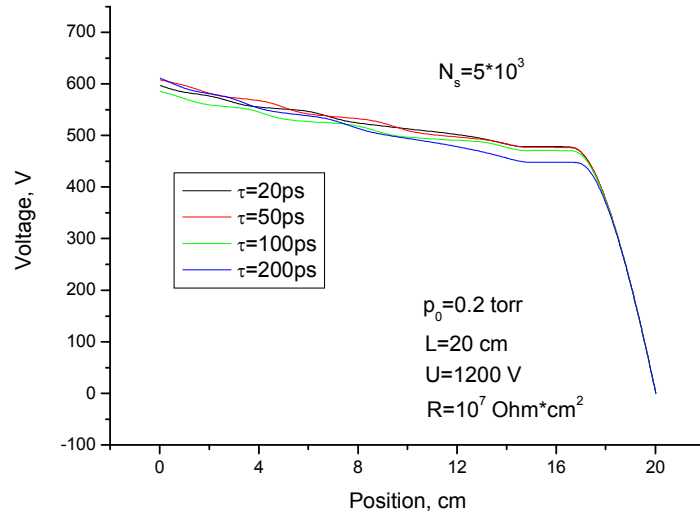


Fig 53.

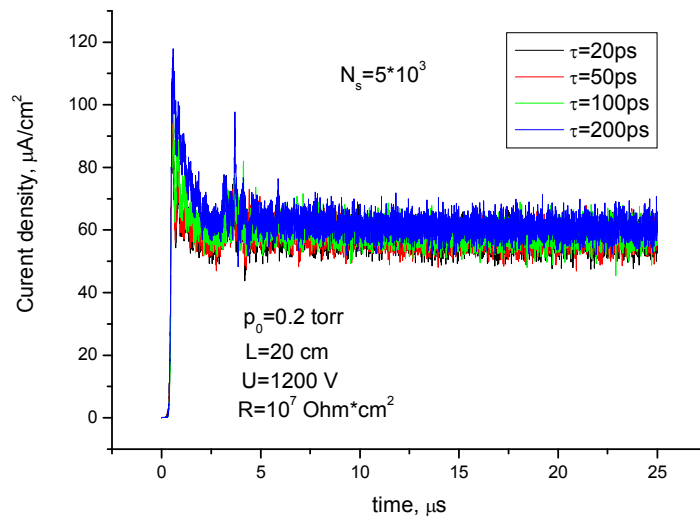


Fig. 54.

1D3V version of PIC-MCC code

When the hard sphere collision model becomes not adequate or relative velocities of colliding particles are not merely defined by projectile particles – it is a good approach for electron-neutral collisions, but it is not the case for electron-electron or ion-ion collisions, - we need to take into consideration the full velocity vector information of colliding particles.

To deduce the velocity vector transformation in the 3V spherical coordinates let us consider an individual collision in the center of mass frame. Let the initial velocity of a projectile particle \vec{v} be defined by two angles α and P as depicted in fig. 55 below (we will use notation of [Birdsall]):

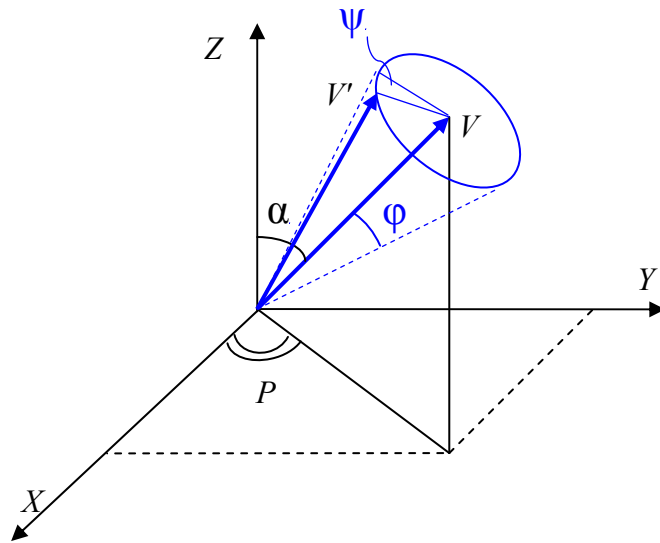


Fig 55

Here:

$$\begin{aligned}
 v_{\perp}^2 &= v_x^2 + v_y^2, & \sin P &= v_y/v_{\perp}, & \cos P &= v_x/v_{\perp} \\
 v^2 &= v_{\perp}^2 + v_z^2, & \sin \alpha &= v_{\perp}/v, & \cos \alpha &= v_z/v
 \end{aligned}$$

Let us consider a frame of reference $OX'Y'Z'$ so that the axis OZ' coincide with \vec{v} and axis OX' lies in the plane OXY . For this reference frame the transformation matrix looks as follows:

$$\Delta = \begin{vmatrix} \sin P & \cos P \cos \alpha & \cos P \sin \alpha \\ -\cos P & \sin P \cos \alpha & \sin P \sin \alpha \\ 0 & -\sin \alpha & \cos \alpha \end{vmatrix}$$

Here we used the property of transformation matrix

$$\Delta = \begin{vmatrix} l_1 & l_2 & l_3 \\ m_1 & m_2 & m_3 \\ n_1 & n_2 & n_3 \end{vmatrix}, \text{ where } l_1 \dots n_3 \text{ are the respective directional cosines, e.g. the}$$

directional cosines of axis OZ' with respect to OX, OY, OZ are (l_3, m_3, n_3) .

The new particle velocity vector will be moved away from old one by the scattering angle φ in the deflection cone at angle ψ . The new components of the velocity in $OX'Y'Z'$ are:

$$\vec{v}' = (v \sin \varphi \cos \psi, v \sin \varphi \sin \psi, v \cos \varphi)$$

In $OXYZ$ frame the velocity component are:

$$v'_x = v [\sin \varphi \cos \psi \sin P + \sin \varphi \sin \psi \cos P \cos \alpha + \cos \varphi \cos P \sin \alpha]$$

$$v'_y = v [-\sin \varphi \cos \psi \cos P + \sin \varphi \sin \psi \sin P \cos \alpha + \cos \varphi \sin P \sin \alpha]$$

$$v'_z = v [0 - \sin \varphi \sin \psi \sin \alpha + \cos \varphi \cos \alpha]$$

(It should be noted that there is a misprint in [Birdsall] in this place).

After that we should transform the velocity back into the lab frame. For example, in general case of elastic collisions of two particles with masses m_α and m_β it is convenient to represent their velocities as follows:

$$\begin{cases} \vec{v}_\alpha = \vec{V}_{cm} + \frac{m_\beta}{m_\alpha + m_\beta} \vec{u} \\ \vec{v}_\beta = \vec{V}_{cm} - \frac{m_\alpha}{m_\alpha + m_\beta} \vec{u} \end{cases}$$

Here:

$$\vec{V}_{cm} = \frac{m_\alpha \vec{v}_\alpha + m_\beta \vec{v}_\beta}{m_\alpha + m_\beta}$$

is the velocity of the center of mass of colliding particles and

$$\vec{u} = \vec{v}_\alpha - \vec{v}_\beta$$

its relative velocity. Because the velocity of the center of mass and $|\vec{u}|$ do not change in collisions we can write the velocities after collision as:

$$\begin{cases} \vec{v}'_\alpha = \vec{v}_\alpha + \frac{m_\beta}{m_\alpha + m_\beta} \Delta \vec{u} \\ \vec{v}'_\beta = \vec{v}_\beta - \frac{m_\alpha}{m_\alpha + m_\beta} \Delta \vec{u} \end{cases}$$

where the components of the vector $\Delta \vec{u} = \vec{u}' - \vec{u}$ are:

$$\Delta u_x = u [\sin \varphi \cos \psi \sin P + \sin \varphi \sin \psi \cos P \cos \alpha + (\cos \varphi - 1) \cos P \sin \alpha]$$

$$\Delta u_y = u [-\sin \varphi \cos \psi \cos P + \sin \varphi \sin \psi \sin P \cos \alpha + (\cos \varphi - 1) \sin P \sin \alpha]$$

$$\Delta u_z = u [-\sin \varphi \sin \psi \sin \alpha + (\cos \varphi - 1) \cos \alpha]$$

These expressions can be simplified by substitution

$$\sin \varphi = 2 \tan \frac{\varphi}{2} / \left(1 + \tan^2 \frac{\varphi}{2} \right)$$

$$1 - \cos \varphi = 2 \tan^2 \frac{\varphi}{2} / \left(1 + \tan^2 \frac{\varphi}{2} \right)$$

Another way is to substitute

$$(\cos \varphi - 1) \rightarrow -2 \sin^2 \frac{\varphi}{2} \quad \text{and} \quad \sin \varphi \rightarrow 2 \sin \frac{\varphi}{2} \cos \frac{\varphi}{2}.$$

It gives:

$$\Delta u_x = 2u \sin \frac{\varphi}{2} \left[\cos \frac{\varphi}{2} \cos \psi \sin P + \cos \frac{\varphi}{2} \sin \psi \cos P \cos \alpha - \sin \frac{\varphi}{2} \cos P \sin \alpha \right]$$

$$\Delta u_y = 2u \sin \frac{\varphi}{2} \left[-\cos \frac{\varphi}{2} \cos \psi \cos P + \cos \frac{\varphi}{2} \sin \psi \sin P \cos \alpha - \sin \frac{\varphi}{2} \sin P \sin \alpha \right]$$

$$\Delta u_z = -2u \sin \frac{\varphi}{2} \left[\cos \frac{\varphi}{2} \sin \psi \sin \alpha + \sin \frac{\varphi}{2} \cos \alpha \right]$$

If $u_{\perp} = 0$:

$$\Delta u_x = u \sin \varphi \cos \psi$$

$$\Delta u_y = u \sin \varphi \sin \psi$$

$$\Delta u_z = u (\cos \varphi - 1)$$

The first test of 3V version of the code was performed for the dark discharge mode. The results of calculation of the drift of a particle in the electric field are well coincide with those for 2V model (Fig. 56):

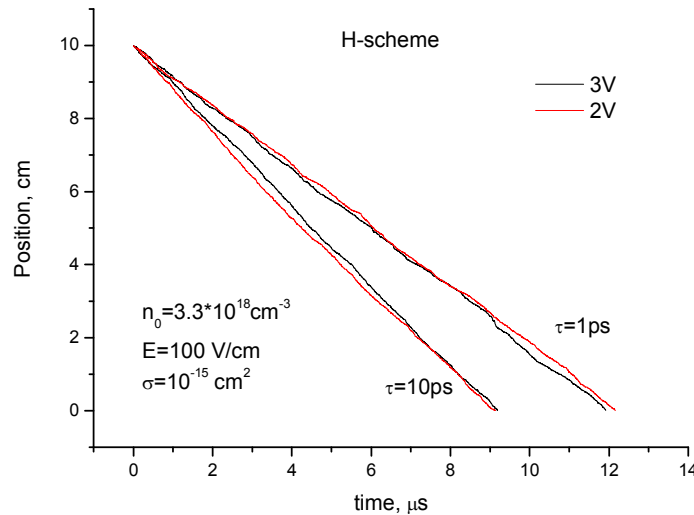


Fig. 56.

Introduction of 3V model in the previous code simulating the DC glow discharge gives a possibility to take into consideration the differential cross-section of electron-neutral ionization collisions.

The energy of scattering electron can be found from a simplified form of this cross-section proposed by [Opal]:

$$E_{scat} = \tilde{E} \tan \left[R \arctan^{-1} \left(\frac{E_{inc} - E_{ion}}{2\tilde{E}} \right) \right]$$

where \tilde{E} is a constant which equals to about 8.3eV for H_2 . The angle ψ as usual is random over 2π and the angle φ now will be defined by equation:

$$\cos \varphi = \frac{2 + E_{scat} - 2(1 + E_{scat})^R}{E_{scat}}$$

The distribution of the scattering angle for different E_{scat} is presented in fig. 57. So the value of $\cos\varphi$ is uniform in (-1,1) only for $E_{scat} \rightarrow 0$ and tends to 1 for large E_{scat} .

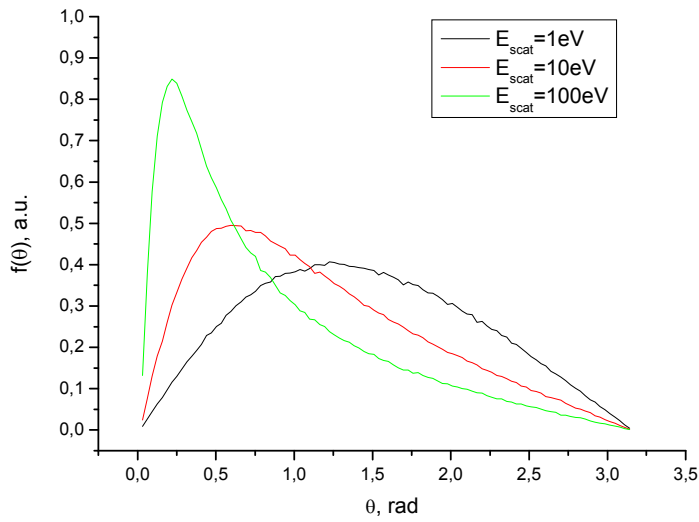


Fig. 57.

The influence of the modification of the ionization cross-section on the results of simulation of the DC glow discharge is shown in figures 58-59. The results obtained are very close to those calculated by 2V version. The made modifications improved somewhat an agreement with experimental data. The value of $d_c=4.9$ cm well coincides now with tabulated value $d_c=5$ cm. The remaining discrepancy in the cathode fall voltage appears to result from the simplification of ionization-recombination and diffusion processes in the simulation of the discharge (in particular, all recombination processes were ignored in calculations).

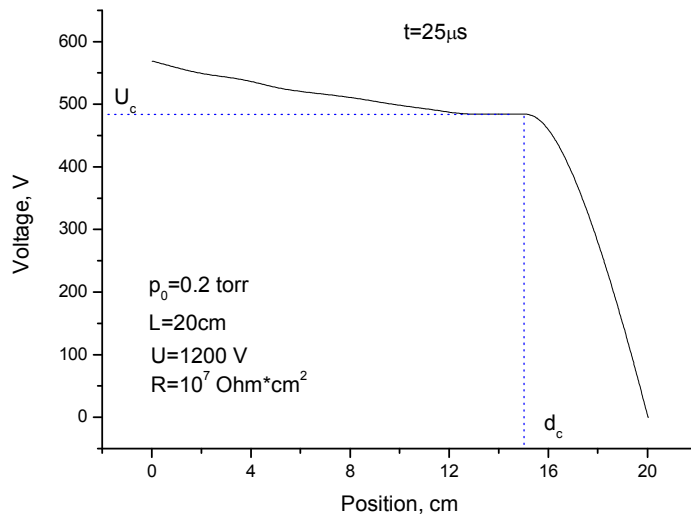


Fig. 58

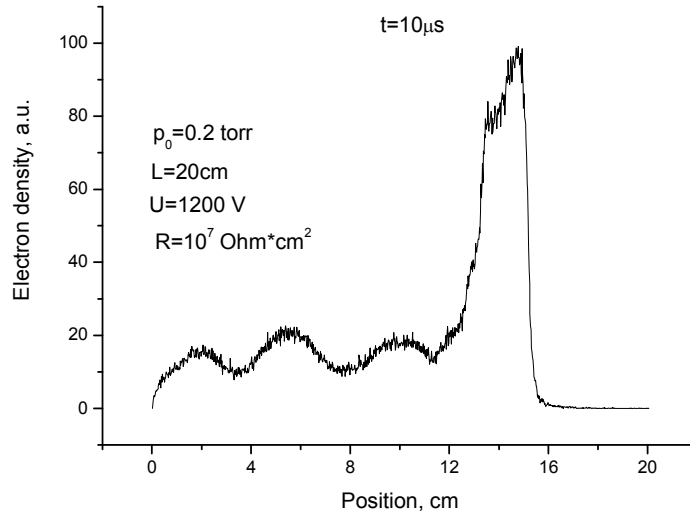


Fig. 59

Lorentz force simulation

Beside the electric field the described 3V model allows to include into consideration the magnetic field. In this case the motion equations to be integrated are

$$\frac{d\vec{x}_i}{dt} = \vec{v}_i \quad m \frac{d\vec{v}_i}{dt} = q(\vec{E} + \vec{v}_i \times \vec{B})$$

and the previous finite-difference approximation moves to

$$\begin{aligned} \vec{x}_i^{n+1} - \vec{x}_i^n &= \vec{v}_i^{n+1/2} dt \\ \vec{v}_i^{n+1/2} - \vec{v}_i^{n-1/2} &= \frac{q}{m} \left[\vec{E}(\vec{x}_i^n) + \frac{(\vec{v}_i^{n+1/2} + \vec{v}_i^{n-1/2})}{2} \times \vec{B}(\vec{x}_i^n) \right] dt \end{aligned}$$

In the most popular algorithm [Boris] splitting the electric and magnetic forces is used. At first we found

$$\vec{v}^- = \vec{v}_i^{n-1/2} + \frac{q}{m} \vec{E}(\vec{x}_i^n)(dt/2)$$

then perform the rotation in accordance with

$$(\vec{v}^+ - \vec{v}^-)/dt = \frac{q}{2m} (\vec{v}^+ + \vec{v}^-) \times \vec{B}(\vec{x}_i^n)$$

and after that, add another part of electric momentum:

$$\vec{v}_i^{n+1/2} = \vec{v}^+ + \frac{q}{m} \vec{E}(\vec{x}_i^n)(dt/2)$$

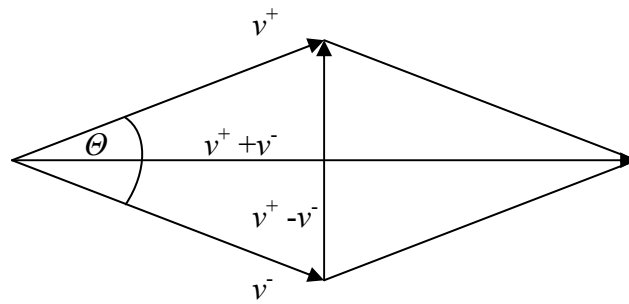


Fig. 60

From the Fig. 60 one can see

$$|\tan \theta/2| = \left| \frac{\vec{v}^+ - \vec{v}^-}{\vec{v}^+ + \vec{v}^-} \right| = \frac{qB}{m} dt/2 = \omega_c dt/2$$

To calculate the vector \vec{v}^+ we should increase the vector \vec{v}^- so that $\vec{v}' \perp (\vec{v}^+ - \vec{v}^-)$ and $\vec{v}' \perp \vec{B}$:

$$\vec{v}' = \vec{v}^- + \vec{v}^- \times \vec{t}$$

where vector \vec{t} equals to (see fig. 61 below)

$$\vec{t} = \frac{q\vec{B}}{m} (dt/2)$$

Finally,

$$\vec{v}^+ = \vec{v}^- + \vec{v}' \times \vec{s}$$

where

$$\vec{s} = 2\vec{t}/(t^2 + 1)$$

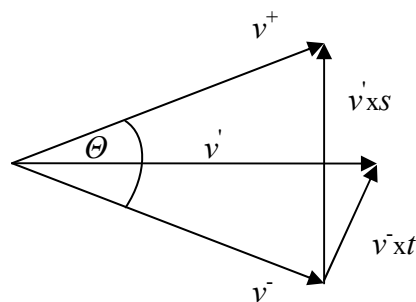


Fig. 61

In particular, if $\vec{B} = (0, 0, B)$ then

$$v'_x = v^-_x + v^-_y t$$

$$v'^+_y = v^-_y - v'_x s$$

$$v_x^+ = v' + v_y^+ t$$

where

$$t = -\tan \theta / 2$$

$$s = -\sin \theta = 2t / (1 + t^2)$$

In case of constant B the value of the time steps dt can be set rather large. So that it would be more preferable to use the direct conversation:

$$\begin{pmatrix} v_x^+ \\ v_y^+ \end{pmatrix} = \begin{pmatrix} \cos \omega_c dt & \sin \omega_c dt \\ -\sin \omega_c dt & \cos \omega_c dt \end{pmatrix} \begin{pmatrix} v_x^- \\ v_y^- \end{pmatrix}$$

The particle's drift in the crossed electric and magnetic fields and the same plasma conditions is presented in fig. 62. The magnetic field was assumed to be directed along X axis. The cyclotron frequency $\omega \approx 1.76 \cdot 10^7 B$ becomes equal to the frequency of electron-atom collisions $\nu_{e0} = \sigma n \langle v \rangle$ when B is about 10kGs. In the case of $B > 20$ kGs all particles are magnetized and make a drift in Y direction with the velocity:

$$v_d = \frac{cE}{B} \cong 10^6 \text{ cm/s (for } B=10\text{kGs)}$$

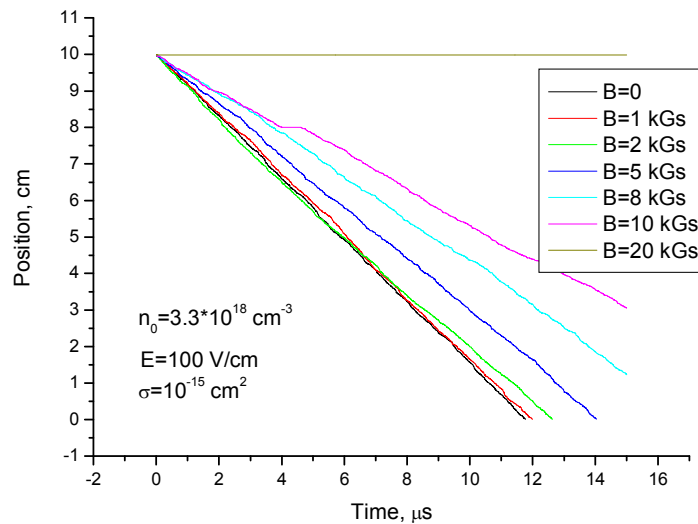


Fig 62. The drift of electrons along Z direction (across magnet field)

Binary collisions in the PIC-MCC code

Up to now our finite-size particle model does not include charged particle collisions. The presented above simulations using Vlasov-Boltzmann equation take into account only long-range collective interactions. But to simulate heating processes, transport and relaxation phenomena we need to introduce into the model electron-electron and electron-ion binary collisions.

There are two ways to include into consideration the short-range interactions. One of them is a hybrid particle-particle – particle mesh (P³M) algorithm developed by [Hockney].

The main point of the technique consists in splitting of long-range forces (e.g. coulombic) onto two parts. The first part (short-range) is calculated by direct summation of forces of binary interactions of a given particle with neighboring ones (particle-particle method). The smooth long-range part of the force is calculated using the particle-mesh approach. The second way is to introduce small-range small-angle binary collisions by Monte Carlo method. It is equivalent to consideration of the kinetic equation with the collision term in the Landau form [Takizuka]. Due the large number of colliding pairs the direct integration of the equation are impractical. Therefore the essential constituent of the algorithm is the rule for selecting of representative pairs of colliding particles.

The last approach is more frequently used in the PIC codes nowadays [Dawson, Ruhl] and so it was chosen for the code in progress. This model can be summarized as follows:

1. For the reason of simplicity it is assumed that only those particles that belong to the same spatial cell of the mesh have collisional interactions.
2. Simultaneous interaction of all possible collision pairs (which total number is $n(n-1)/2$) is approximated by the only one randomly selected pair (which total number - $n/2$).
3. The post-collision momenta of particles in each selected pair are determined with the help of the kinematic relations of binary collisions described in the previous section. The distribution of angle φ follows the Spitzer formula for small-angle scattering; angle ψ is chosen randomly with uniform distribution in $(0, 2\pi)$.
4. Collisions between different species are assumed to occur successively.
5. Particle acceleration and collisions are considered to be uncoupled.

To realize the algorithm we need at first to determine particles that overlap in a given spatial cell. It is easily done using the well known linked-list structure during charge weighting. After that it is necessary to select (in a random way) the representative particle pairs from all possible collision pairs as illustrated in figure 63:

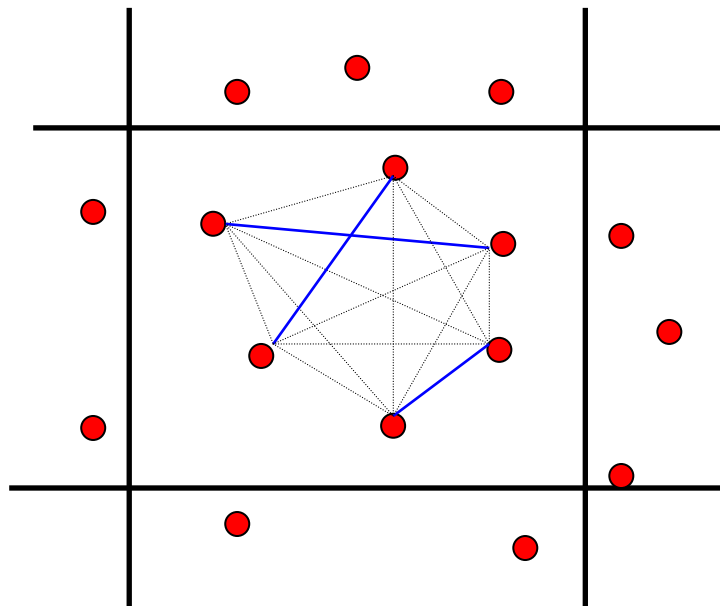


Fig. 63.

This selection is performed using indirect addressing and uniformly distributed random permutations as shown in fig. 64. Pairing of even number like particles is trivial. In case of odd number of particles the first tree of them is combined in three pairs. Because each of them undergoes twice as many collisions as other particles the respective collision frequencies are divided by two. Due to indirect addressing pairing of unlike particles is very similar. If $n_\alpha > n_\beta$ we selected n_α pairs filling even addresses with α particles and odd addresses – with β particles. As soon as the β particles are exhausted we repeat scanning β particles from the beginning until all vacant odd addresses are filled. For the permutations Fischer’s algorithm is used [Knuth].

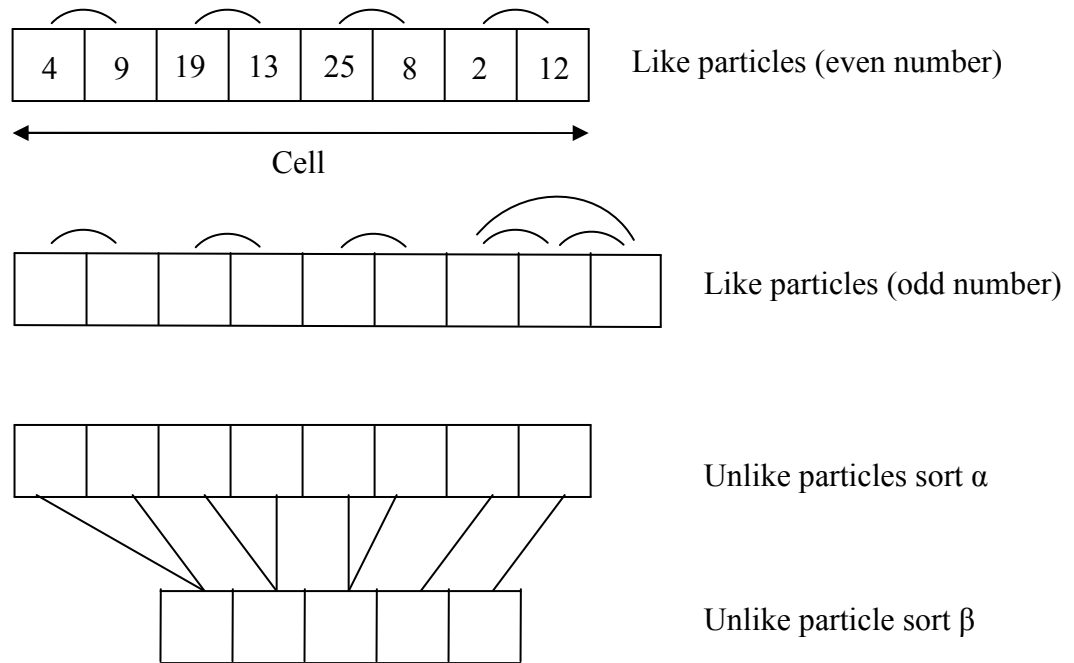


Fig. 64. The pairing rules

The Spitzer formula defines that the differential probability for scattering of α particle on a target β in the angle $(\varphi, \varphi + d\varphi)$ in a time Δt is:

$$P(\varphi)d\varphi = \exp\left(-\frac{\varphi^2}{2v_{\alpha\beta}\Delta t}\right) \frac{\varphi}{v_{\alpha\beta}\Delta t} d\varphi$$

where

$$v_{\alpha\beta} = \frac{4\pi e_\alpha^2 e_\beta^2 n_\beta}{m_\alpha u^3} \Lambda$$

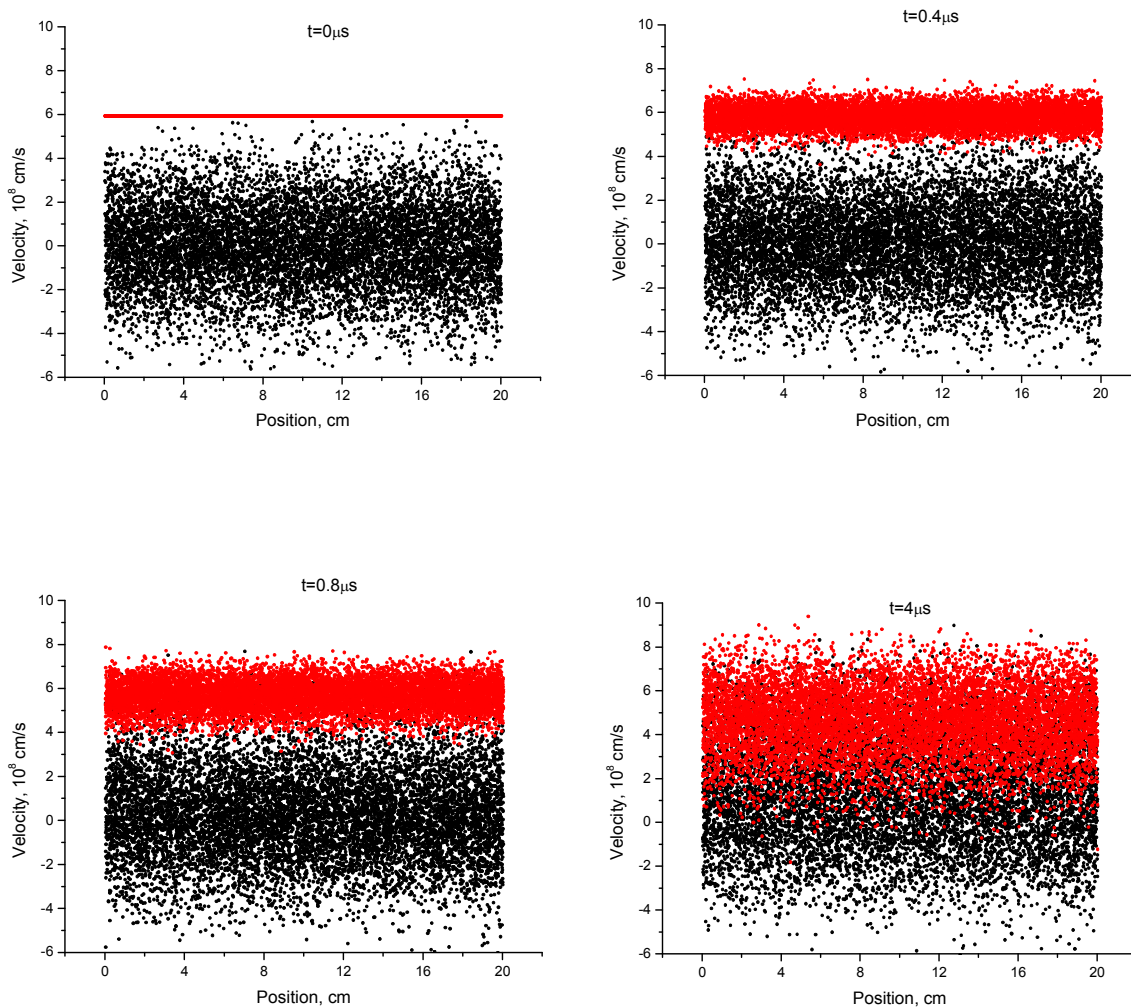
characterizes an angular relaxation rate of a particle α in the field of β particles. It is frequently referenced as a collision frequency. (Here $u = v_\alpha - v_\beta$ is the relative velocity of

colliding particles, e_α , e_β - their charges, $m_{\alpha\beta} = \frac{m_\alpha m_\beta}{m_\alpha + m_\beta}$ - their reduced mass and Λ is the Coulomb logarithm). It gives a possibility to choose the scattering angle φ in accordance the following equation:

$$\varphi = \sqrt{-2v_{\alpha\beta}\Delta t \ln(1-R)}$$

It should be noted that using the presented algorithm of particle pairing in case of unlike particles $\min\{n_\alpha, n_\beta\}$ is to be used as n_β in the expression for collision frequency.

As an example in figures below one can see scattering of the electron beam with energy 100 eV in plasma with density $n=10^{12}\text{cm}^{-3}$ and initial temperature 20 eV due to electron-electron collision only. Relaxation time under this plasma conditions $\tau_{\alpha\beta}=1/\nu_{\alpha\beta}\approx 12\mu\text{s}$.



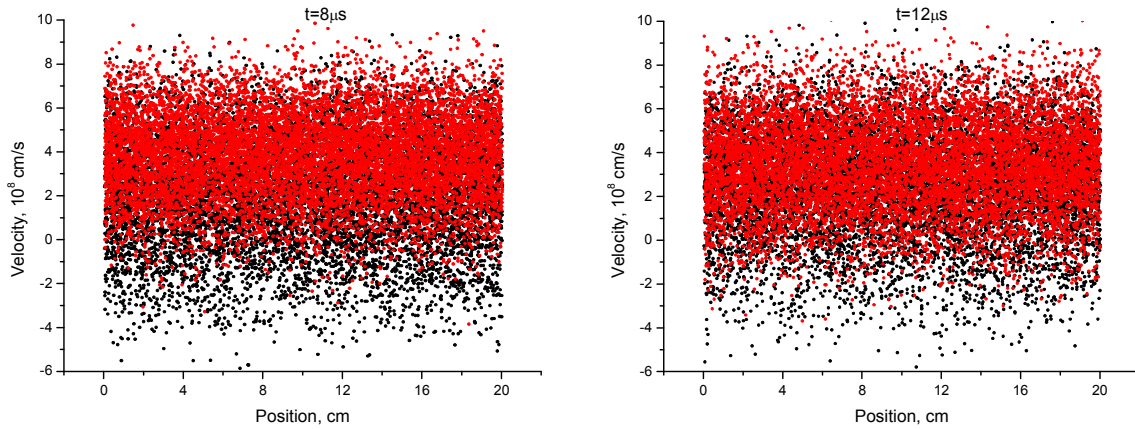
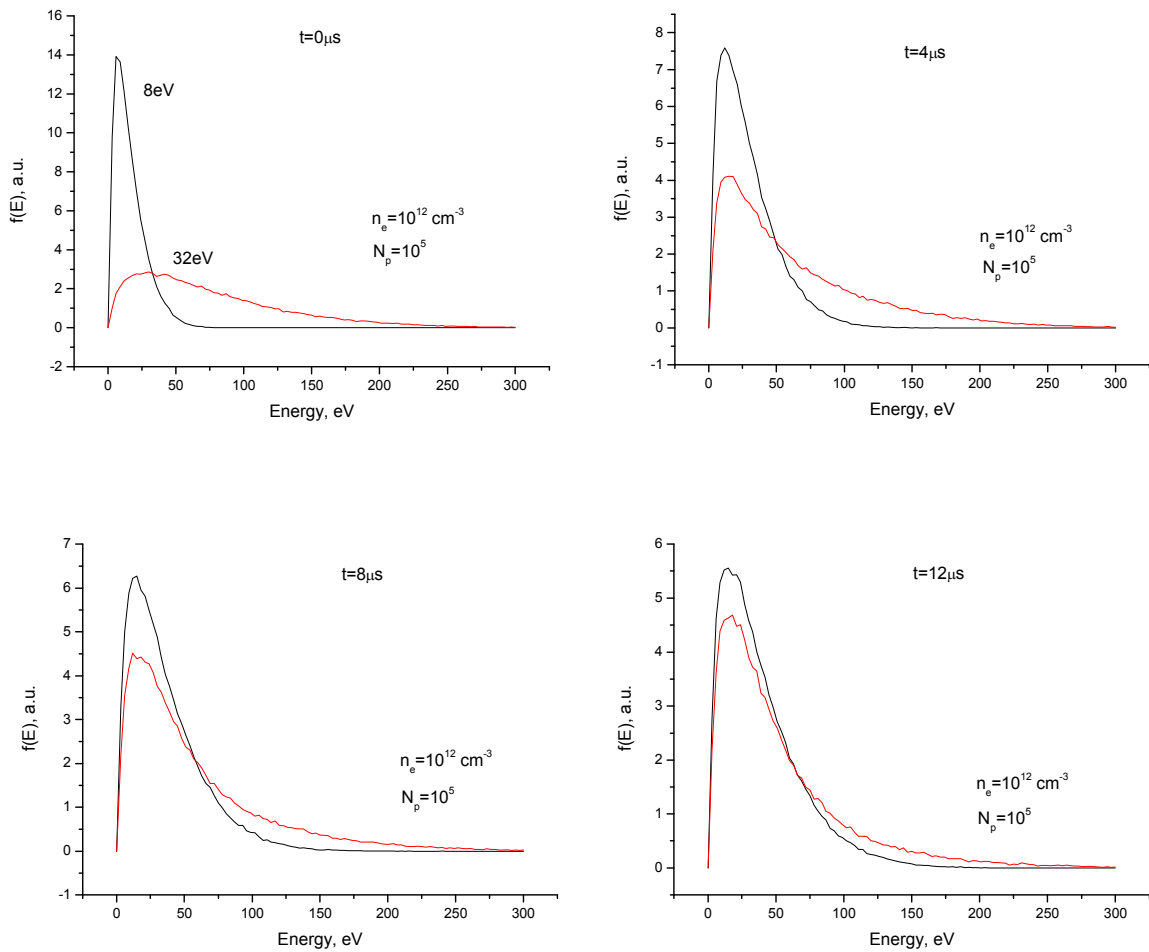


Fig 65

The relaxation of two temperature electron distribution is presented in fig. 66. The plasma was considered to be consisted of two groups of the particles with maxwellian velocity distribution. The first one has the temperature 8eV, the second one – 32 eV. In this case the energy relaxation time is $\tau_{\alpha\beta}=1/\nu_{\alpha\beta}\approx 17\mu\text{s}$.



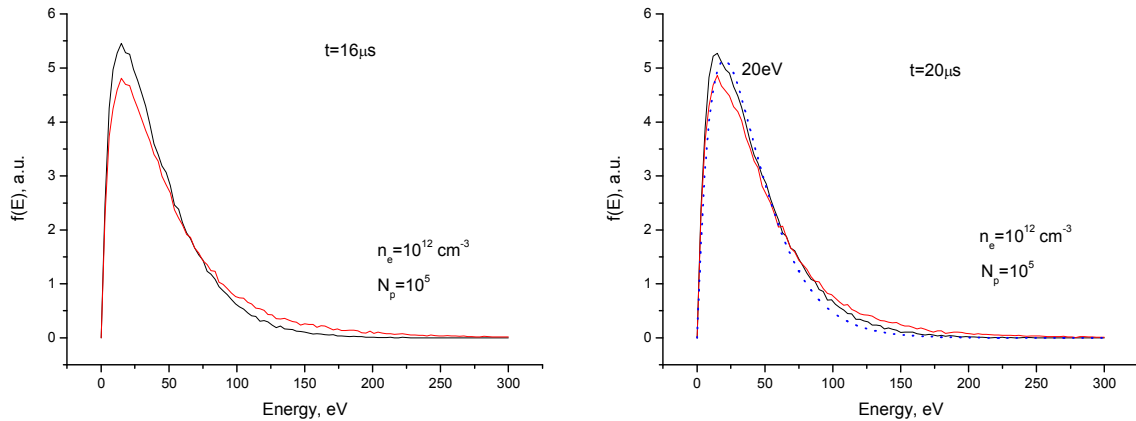


Fig. 66. Temperature relaxation.
(Dotted line represents Maxwell distribution)

References

1. R.W. Hockney and J.W. Eastwood, *Computer Simulation Using Particles*, New York: McGraw-Hill, 1981
2. C.K. Birdsall and A.B. Langdon, *Plasma Physics via Computer Simulation*, New York: McGraw-Hill, 1985
3. H. Tawara et al, *J. Phys. Chem. Ref. Data*, v. 19, p.617-636 (1990).
4. P.Burger, *Phys. Fluids*, v. 10, p. 658-666 (1967)
5. C.B. Opal, W.K. Peterson and E.C. Beaty, *J. Chem. Phys.*, v. 55, p. 4100-4106 (1971)
6. J. P. Boris, K.V. Roberts, *J. Comput. Phys*, v. 4, p. 552-571 (1969)
7. T. Takizuka and H. Abe, *J. Comput. Phys*, v. 25, p. 205-219 (1977)
8. J.M. Dawson, S. Ma, R.D. Sydora, *Comput. Phys. Commun.*, v. 77, p. 190- (1993)
9. H. Ruhl, *Classical Particle Simulations with PSC code*, Bochum, 2005
10. D. E. Knuth, *The Art of Computer Programming*, London: Eddison-Wesley Publ. Co., 1981

Acknowledgements

We acknowledge the support of the European Community-Research Infrastructure Activity under the FP6 “Structuring the European Research Area” programme (CARE, contract number RII3-CT-2003-506395)